



Deposited via The University of Leeds.

White Rose Research Online URL for this paper:

<https://eprints.whiterose.ac.uk/id/eprint/228925/>

Version: Accepted Version

---

**Article:**

Cao, Y., Zhang, M., Huang, J. et al. (2025) Load-Transfer Suspended Backpack With Bioinspired Vibration Isolation for Shoulder Pressure Reduction Across Diverse Terrains. IEEE Transactions on Robotics, 41. pp. 3059-3077. ISSN: 1552-3098

<https://doi.org/10.1109/tro.2025.3562488>

---

© 2025 IEEE. Personal use of this material is permitted. Permission from IEEE must be obtained for all other uses, in any current or future media, including reprinting/republishing this material for advertising or promotional purposes, creating new collective works, for resale or redistribution to servers or lists, or reuse of any copyrighted component of this work in other works.

**Reuse**

Items deposited in White Rose Research Online are protected by copyright, with all rights reserved unless indicated otherwise. They may be downloaded and/or printed for private study, or other acts as permitted by national copyright laws. The publisher or other rights holders may allow further reproduction and re-use of the full text version. This is indicated by the licence information on the White Rose Research Online record for the item.

**Takedown**

If you consider content in White Rose Research Online to be in breach of UK law, please notify us by emailing [eprints@whiterose.ac.uk](mailto:eprints@whiterose.ac.uk) including the URL of the record and the reason for the withdrawal request.

# Load-transfer Suspended Backpack with Bio-inspired Vibration Isolation for Shoulder Pressure Reduction Across Diverse Terrains

Yu Cao, *Member, IEEE*, Mengshi Zhang, Jian Huang, *Senior Member, IEEE*, Samer Mohammed, *Senior Member, IEEE*

**Abstract**—Active suspended backpacks represent a promising solution to mitigate the impact of inertial forces on individuals engaged in load carriage. However, identifying effective control objectives aimed at enhancing human carrying capacity remains a significant challenge. In this study, we introduce a novel approach by integrating a limb-like structure-type (LLS) bio-inspired vibration isolator, modeled using Lagrangian mechanics, into an active load-transfer suspended backpack to primarily alleviate human shoulder pressure, thereby constructing a human-robot interaction control framework for the system. Drawing from a double-mass coupled oscillator model, this approach formulates a vertical dynamics model for the human-backpack system, systematically exploring the principles of both static load transfer and dynamic load reduction on the human shoulder. Subsequently, a series elastic actuators-based controller with prescribed performance is proposed to simultaneously achieve trajectory tracking and ensure load motion within the limited range. Theoretically, we validate the input-output stability of the LLS model and guarantee the ultimate uniform boundedness of the closed-loop system. Simulation and experimental trials conducted across different terrain scenarios validate the effectiveness of the proposed method, highlighting reductions of 18.68% in metabolic rate during level ground walking, 9.58% in a staircase scenario and 12.35% in a complex terrain, involving uphill, downstairs, and flat ground walking.

**Index Terms**—Active load-transfer backpack, bio-inspired vibration isolation, series elastic actuators-based controller, various terrain scenarios.

## I. INTRODUCTION

**D**URING human carriage, the vertical movement of the hip results in the acceleration of a loaded backpack with

This work was supported in part by National Natural Science Foundation of China under Grant 62333007, U24A20280, and 62103157, in part by U.K. Research and Innovation (UKRI) Horizon Europe Guarantee under Grant EP/Z001234/1, in part by Knowledge Innovation Program of Wuhan-Basic Research under Grant No. 2023010201010055. (*Corresponding author: Jian Huang*)

Y. Cao was affiliated with the Hubei Key Laboratory of Brain-inspired Intelligent Systems, School of Artificial Intelligence and Automation, Huazhong University of Science & Technology, Wuhan, China during the research and is currently with the School of Electronic & Electrical Engineering, University of Leeds, Leeds, UK. (e-mail: y.cao1@leeds.ac.uk)

J. Huang is with the Hubei Key Laboratory of Brain-inspired Intelligent Systems, School of Artificial Intelligence and Automation, Huazhong University of Science and Technology, Wuhan, China. (e-mail: huang\_jan@mail.hust.edu.cn)

M. Zhang is with Wuhan United Imaging Healthcare Surgical Technology Co., Ltd., Wuhan, China (e-mail: mengshi521@vip.qq.com)

S. Mohammed is with Univ Paris Est Creteil, LISSI, F-94400 Vitry, France. (e-mail: samer.mohammed@u-pec.fr)

each step, subjecting the wearer to significant peak forces [1], [2]. To address this issue, enhancing overall metabolic efficiency during load carriage can be achieved through introducing compliance [3]–[5]. This concept inspired Rome et al. to suspend loads from a backpack frame, reducing peak vertical force and the energy cost of walking through the utilization of bungee cords [6]. Over subsequent decades of development, a variety of suspended backpack designs have emerged. Classified by actuation type, these devices generally fall into three categories: passive, semi-active, and active [7]. Passive suspended backpacks integrate elements like springs or dampers to provide compliance [8]–[10]. These components function as linear vibration isolators, reducing peak shoulder forces and vertical ground forces while enhancing metabolic efficiency [11]. However, backpacks without external power input often have fixed stiffness and damping, presenting challenges in adapting to diverse movement speeds and terrains. For this problem, semi-active suspended backpacks incorporate controlled dampers to attenuate load vibration [12]–[14], yet the complex characteristics of dampers such as hysteresis, non-linearity, and limited bandwidth typically hinder real-time adaptation to users' gait. In contrast, active suspended backpacks offer active load regulation [15]–[17], featuring high bandwidth and wide adaptability. This enables dynamic modulation of the system's equivalent stiffness and damping, effectively addressing challenges posed by the previous two types of suspended backpacks.

Within the field of active backpacks, the central aim is to design a control strategy that effectively reduces peak force (PF) or peak acceleration (PA). A straightforward approach involves exerting a reverse force, applying the system's full states (including both absolute position and velocity), with goal of maintaining a relatively constant absolute position and zero acceleration [15]. Park et al. [18] introduced a switch force controller based on over-zero detection of the human body's vertical acceleration. Yang et al. [19] adopted a different approach, establishing a correlation between the backpack's equivalent stiffness and damping and the load's work, thereby generating higher-level directives using a bipedal impulsive model of human walking [20]. However, the approaches often require accurate vertical displacement estimation of human gait and suffer from overall discontinuous control inputs, which may lead to undesirable chattering effects and potentially induce system instability, significantly limiting the

applicability of active suspended backpacks. Notably, current research predominantly concentrates on reducing PA in stationary scenarios, with limited exploration of multi-scenario applications, such as walking on slopes and stairs. Therefore, the ongoing challenge lies in designing a control method that seamlessly adapts to diverse scenarios while ensuring overall system stability and safety.

Given the linear vibration isolator's role in reducing shoulder pressure and improving metabolic efficiency, employing isolators with superior vibration isolation performance could effectively address the aforementioned challenges. Limb-like structure (LLS) bio-inspired vibration isolators, originated from the shape of a crane leg [21], outperform traditional linear isolators in dynamic and complex environments [22]. This presents a novel perspective for enhancing the performance of suspended backpacks in various load-carrying scenarios. Characterized by nonlinear stiffness, nonlinear damping, and nonlinear inertia individually or simultaneously [23], LLS-type bio-inspired isolators provide advantages such as large displacement travel, low resonant frequency, and strong adaptability to high-static-low-dynamic-stiffness (HSLDS) characteristics. These properties enable effective shock absorption and vibration suppression, making them particularly well-suited for suspended backpacks. By reducing load vibrations, the isolators can lower peak shoulder pressure and improve human metabolic efficiency during load carriage across various terrains. Bian et al. explored the damping properties of the LLS, revealing nonlinear damping effects that effectively adapt to vibration displacements and frequencies [24]. Niu et al. presented a compliant LLS that showed robust stability and a pronounced HSLDS characteristic, simultaneously [25]. Zhang et al. introduced a neural network control for active suspensions employing bioinspired dynamics to improve vibration suppression and energy efficiency while addressing input delay and uncertainties [26]. Hu et al. proposed an approximation-free control using bioinspired models for uncertain suspension systems, enhancing vibration suppression and reducing computational burden [27]. Pan et al. considered the vibrations as additional perturbations and guaranteed the boundedness of the LLS system for nonlinear suspension systems and highlighted the energy saving properties [28]. However, to the best of our knowledge, bio-inspired vibration isolators have not yet been applied to suspended backpacks. Additionally, the stability analysis of these isolators usually focuses on uniform ultimate boundedness, emphasizing long-term behavior rather than the direct relationship between excitations and responses, leading to a less intuitive description of system stability.

As previously mentioned, suspended backpacks have primarily focused on mitigating PA/PF, yet the load mass still imposes a significant strain on human shoulders [29]. Load transfer emerges as a practical alternative. Typically, there are two options for load transfer: weight transfer to the ground and transfer to the lower extremities [30]. Concerning the former, exoskeletons and supernumerary robotic limbs (SRLs) stand as typical robotic devices. Wang et al. [31] designed a lower extremity exoskeleton for passive body weight support to reduce load on the knee. Dijk et al. [32] and Zhou et al. [33] designed exoskeleton-like legs attached to the human foot's

heel, directing weight to the ground through a force pathway. Ming et al. [34] proposed an SRL for weight transfer through rigid robotic mechanisms. However, exoskeleton inertia often alters natural human gait, unintentionally increasing load carrying inefficiency [35]. SRLs, on the other hand, involve additional mechanisms that require advanced controllers for load transfer, posing challenges for real-world implementation. Regarding the latter approach, relying on the lower extremities offers a relatively simple solution, capitalizing on the muscularity present. Park et al. designed a secondary spine to transfer loads from human shoulders to pelvis [36]. They further refined this by introducing load-bearing columns attached to a suspended backpack, enabling load distribution between human shoulders and pelvis [18]. However, such supplementary passive structures often introduce complexity, leading to challenges in designing a unified control framework for shoulder pressure regulation.

Also, it is critical for the active backpack system to operate within the designated load travel range, as any deviation could lead to potential collisions with physical limits. Traditional controllers have predominantly centered around ensuring steady-state performance, often neglecting the necessity of securing guaranteed transient performance. Further exploration into studying comprehensive state constraints throughout the system remains crucial. A promising direction for addressing this challenge is through the adoption of prescribed performance control (PPC) [37]. This method involves transforming a constrained system into an equivalent unconstrained one by designing error transformation and constraint functions [38], [39]. The primary goal of PPC is to ensure both transient and steady-state performance, with a specific emphasis on establishing output constraints. Zheng et al. introduced a prescribed performance controller with a disturbance observer to ensure the microrobot's continuous visibility within the scope of microscopic cameras [40]. Cao et al. applied the concept of prescribed performance to achieve position-constrained "assist-as-needed" control for rehabilitation robots [41]. Papa-georgiou et al. applied PPC to enhance the performance of a passive physical human-robot interaction (pHRI) controller [42]. Despite its widespread use, to the best of our knowledge, this approach has yet to be implemented in the context of active suspended backpacks.

In this study, we have developed a compact active load-transfer backpack that serves the dual purpose of transferring static loads while mitigating PA/PF. This innovation targets the reduction of shoulder pressure and the enhancement of metabolic efficiency across various walking scenarios. The backpack features separate panels to facilitate load sharing between human shoulders and pelvis. Through an analysis of static load transfer and dynamic load reduction, we have reframed the challenge of reducing shoulder pressure through the integration of a Lagrangian-based LLS-type bio-inspired vibration isolator and load-transfer positional offsets to generate the desired trajectory. Subsequently, we introduce a series elastic actuators (SEA)-based controller with prescribed performance to attain trajectory tracking and ensure the load operates within the designated range. The contribution of this paper can be summarized as follows: 1) The incorporation

of a separated panel design in the backpack successfully facilitated the transfer of both static and dynamic loads from the shoulders to pelvis; 2) A novel Lagrangian-based LLS-type bio-inspired vibration isolator was introduced to enable the backpack to adapt to various terrains, highlighting its input-output stability. To the best of our knowledge, this is the first attempt to apply this technique to active suspended backpacks; 3) A new SEA-based controller with prescribed performance was proposed to address the tracking problem with output constraints; 4) A comprehensive set of multi-scenario simulations and experiments were conducted to validate the efficacy of the proposed method, including dynamic scenarios such as level-ground, climbing/descending stairs, as well as complex terrains including level-ground, stairs, and ramps.

We have evolved our conference paper [16] to offer a more comprehensive and impactful study in this journal version. While the conference version concentrated primarily on the impedance controller (essentially a linear vibration isolator), this evolved paper introduces a novel LLS-type bio-inspired vibration isolator, modeled using Lagrangian mechanics (presented as a nonlinear vibration isolator). This innovative advancement effectively addresses the challenges of applying the suspended backpack across different terrains. The evolved version includes a substantial extension of content, covering various critical aspects. Firstly, we expound upon the motion control framework, extending its capabilities to concurrently reduce both dynamic and static loads beyond the conference version. The load transfer principle and the bio-inspired vibration isolator collaborate to generate the desired trajectory, while the SEA-based controller with position constraints ensures accurate tracking. Secondly, we propose the implementation of a LLS-type bio-inspired vibration isolator to dynamically adjust the backpack's motion in response to varying walking speeds and terrains, whereas the linear vibration isolator used in the conference version struggles to accommodate the challenges posed by complex terrains. Also, we provide a theoretical demonstration of the input-output stability of the bio-inspired vibration isolator. This innovation not only addresses the constrained performance of the linear vibration isolator from the conference version but also establishes a theoretical foundation for ensuring the global stability of the system. Finally, in contrast to the conference version, which conducted experiments solely at a fixed speed on a treadmill, this paper goes beyond by showcasing the enhanced performance through various simulation and experiments across diverse terrains. The results not only demonstrate the adaptability of the proposed method to various terrains but also highlight its superior efficiency in optimizing human metabolic rate compared to existing methods.

The paper is organized as follows. Section II introduces the load-transfer backpack system, its dynamics, and evaluation methods. In Section III, we explore the load transfer principles, followed by an in-depth analysis of the LLS-type bio-inspired vibration isolator. Moving to Section IV, we introduce the SEA-based controller with prescribed performance. Sections V and VI includes discussions on simulations and experimental findings. Finally, Section VII summarizes our conclusions and outlines potential avenues for future research.

## II. SYSTEM MODELING

Fig. 1 illustrates a schematic depiction of an individual wearing a load-transfer backpack. The load-backpack configuration comprises three panels: panel 1, fastened to the shoulder via shoulder straps; panel 3, affixed to the wearer's waist using waist belts to ensure ample static friction; and the load secured onto panel 2. Concurrently, panel 1 and panel 2 are interconnected by a set of parallel springs, functioning as shoulder springs (SSs); while panel 2 and panel 3 are interconnected by a series of springs and a linear actuator, forming a spring-bearing-spring (SBS) arrangement. Consequently, the combined support of panel 1 and panel 3 sustains panel 2, with the load distribution between panel 1 and panel 3 adjustable through motor actuation, facilitating the transfer of load from the shoulders to the pelvis.

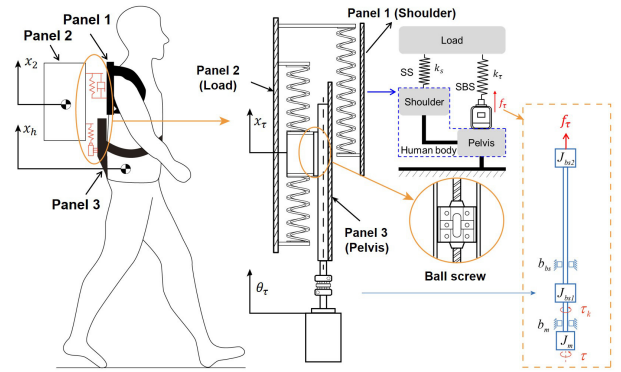


Fig. 1. Schematic view of human load carriage through a load-transfer backpack.

### A. Dynamics

As the subject walks, the load undergoes periodic acceleration. Based on the principles of static equilibrium, the vertical motion of panel 2 is depicted in Fig. 2 and is mathematically formulated as follows:

$$m_2 \ddot{x}_2 = -k_s x_\rho - c_s \dot{x}_\rho + k_r (x_\tau - x_2) - m_2 g + \nu_2 \quad (1)$$

where  $x_\rho = x_2 - x_1$ .  $x_1$ ,  $x_2$  and  $x_\tau$  are the vertical displacement of panel 1, panel 2 and the ball screw of the linear actuator.  $m_2$  is total weight of the load and panel 2.  $k_s$  and  $c_s$  are the stiffness and damping of SS.  $k_r$  is the stiffness of springs in the SBS.  $\nu_2$  represents the lumped disturbance term in panel 2, including the damping term of the SBS and uncertainties caused by modeling inaccuracies.

Similarly, the dynamics of panel 1 is:

$$m_1 \ddot{x}_1 = k_s x_\rho + c_s \dot{x}_\rho - f_e - m_1 g + \nu_1 \quad (2)$$

where  $f_e$  is the human-robot interaction force at the shoulders which is also the shoulder pressure, denoted as  $f_e = k_f (x_1 - x_h) + c_f (\dot{x}_1 - \dot{x}_h)$ .  $m_1$  is the total weight of panel 1, SSs and mechanical connectors.  $x_h$  is the vertical displacement of the subject's center of gravity (COG).  $\nu_1$  represents the uncertainties caused by modeling inaccuracies in panel 1.

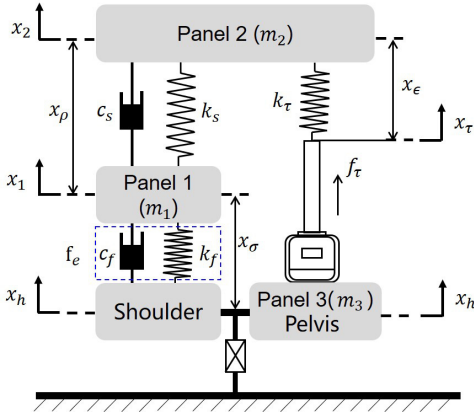


Fig. 2. Schematic dynamics of human-backpack system.

Concerning the linear actuator, the dynamics governing the motor actuation can be described as follows:

$$J_m \ddot{\theta} + b_m \dot{\theta} + l_b k_\tau (x_\tau - x_2) = \tau + \nu_m \quad (3)$$

where  $\tau = k_u i$ , with  $k_u$  representing the torque constant and  $i$  denoting the motor current.  $J_m$  stands for the moment of inertia, while  $b_m$  corresponds to the damping.  $l_b$  signifies the lead of the ball screw.  $\nu_m$  denotes the lumped disturbance term, including the damping term of the SBS and the uncertainties caused by modeling inaccuracies.

Given that the positions of both panel 3 and the human pelvis remain relatively fixed due to static friction, the core principle of load transfer entails the human pelvis shouldering the reactive force of the motor output. This foundational concept can be represented as follows:

$$f_h = f_\tau + m_3 \ddot{x}_h \quad (4)$$

where  $f_h$  is the static friction between panel 3 and human pelvis.  $f_\tau = \frac{1}{l_b} \tau$  is the output of the linear actuator.  $m_3$  is the total weight of panel 3, including a motor and a linear actuator.

Considering the vertical position of the ball screw, we have the following relationship:

$$\begin{cases} x_\tau - x_h = l_b \theta, \\ x_{h2} = x_2 - x_h = x_\rho + x_\sigma \\ x_2 - x_\tau = (x_2 - x_h) - (x_\tau - x_h) = x_{h2} - l_b \theta \end{cases} \quad (5)$$

where  $x_\sigma = x_1 - x_h$ . The dynamics of the human-backpack can be rewritten as:

$$m_2 \ddot{x}_\rho + c_\rho \dot{x}_\rho + k_\rho x_\rho + k_\tau (x_{h2} - l_b \theta) = f_\rho + \nu_\rho \quad (6)$$

$$J \ddot{\theta} + b \dot{\theta} + k_\tau (l_b \theta - x_{h2}) = f_\tau + \nu_\tau \quad (7)$$

where  $m_{21} = \frac{m_2}{m_1}$ ,  $c_\rho = (1 + m_{21})c_s$ ,  $k_\rho = (1 + m_{21})k_s$ ,  $f_\rho = m_{21}f_e$ ,  $J = \frac{1}{l_b} J_m$ ,  $b = \frac{1}{l_b} b_m$ ,  $\nu_\rho = \nu_2 - m_{21}\nu_1$ , and  $\nu_\tau = \nu_m/l_b$ . This embodies a standard SEA model, leveraging the potential benefits of relative displacements between panels to articulate the system's states, rather than relying on the often intricate and real-time challenging measurement of  $x_h$ .

## B. Performance Evaluation

The evaluation includes three distinct metrics: shoulder pressure, load acceleration, and metabolic reduction. These metrics individually depict the system's performance from the standpoint of both the human body and the backpack. These metrics collectively provide a comprehensive portrayal of the system's capabilities, illuminating its potential to elevate the efficiency of human load carriage.

1) *Shoulder Pressure*: The assessment of shoulder pressure  $f_e$  involves the utilization of a soft ballonet affixed to the shoulder strap. Through the introduction of a specific quantity of air mass, the external pressures on the shoulder are determined by employing a technique described in [43].

2) *Load Peak Acceleration*: The inertial force introduces an augmented dynamic load on the human shoulder. To quantify this impact, we present the maximum absolute value of the load's vertical acceleration as quantitative indicators, given by

$$\text{MAX}(\ddot{x}_2) = \max(|\ddot{x}_2|) \quad (8)$$

3) *Metabolic Reduction*: The human metabolic energy was evaluated by a wearable metabolic system (K5, COSMED, Italy). Only trails with Respiratory Exchange Ratio (RER)  $\leq 1$  were recorded, and the gross metabolic rate was normalized to each participant's body mass. Details can be found in the experimental section.

## III. REFERENCE TRAJECTORY GENERATION

The objective of this section is to generate a desired trajectory for the SEA-based controller based on the principles of static load transfer and dynamic load alleviation.

### A. Static Load Transfer

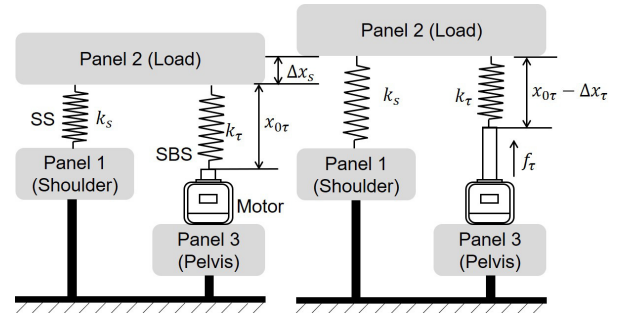


Fig. 3. Idea of load transfer.

When a subject remains stationary with the loaded backpack, the vertical positions of panel 1 and panel 3 remain fixed in relation to the ground, as illustrated in Fig. 3. The load experiences the effects of gravity  $m_2 g$ , the spring's elastic force  $f_s$ , and the motor actuation  $f_\tau$  simultaneously. Upon the motor generating an upward force  $f_\tau$ , the spring within the SBS results in a compressive displacement  $\Delta x_\tau$ , while the SS initiates a restorative displacement  $\Delta x_s$ . This action redistributes the load between the shoulders and pelvis.

Notably, the restorative force  $f_s$  equates the driving force  $f_\tau$ , thus conforming to the following relationship:

$$f_s = f_\tau = k_s \Delta x_s = k_\tau \Delta x_\tau, \Delta x_\tau = \frac{k_s}{k_\tau} \Delta x_s \quad (9)$$

This signifies a partial transfer of the load from the shoulder to pelvis. The magnitude of  $\Delta x_\tau$  holds the capacity to control  $\Delta x_s$ , consequently dictating the proportion of load transfer from the shoulder to pelvis. This distribution can be quantified by:

$$0 \leq \xi = k_s \frac{\Delta x_s}{m_2 g} = k_\tau \frac{\Delta x_\tau}{m_2 g} \leq 1 \quad (10)$$

where  $\xi$  denotes the load transfer percentage, i.e.,  $\xi = 0\%$  indicates no load is transferred from the shoulders to pelvis, and  $\xi = 100\%$  means the motor output counteracts the gravity of the load.

This perspective enables the distribution of the load between the human shoulder and pelvis by setting a desired transfer ratio  $\xi_d$ , irrespective of the terrain in which the human-backpack system operates. Subsequently, a position  $\Delta x_{sd}$  can be generated from  $\xi_d$ , given by

$$\Delta x_{sd} = \frac{\xi_d}{k_s} m_2 g \quad (11)$$

Consequently, as the motor drive actuates the load to track this predetermined setpoint, the load's mass is distributed between the shoulders and pelvis, facilitating static load transfer.

*Remark 1:* Load transfer heavily relies on the motor's capabilities. Transferring the entire load to the pelvis requires the motor to generate greater driving force, necessitating increased motor power and higher-capacity battery, which leads to the increment of the overall system mass. Additionally, load transfer is influenced by the static friction between the human waist and the pack's waist belt. Excessive load transfer may exceed the maximum static friction threshold, potentially reducing effectiveness. Therefore, the factors mentioned above lead us to choose partial load transfer over full load transfer.

*Remark 2:* The metabolic energy expenditure during human carriage is influenced by subjective and objective factors, including cardiovascular function, movement coordination, stability, and individual carriage experience, etc [44] [45]. Currently, there is no widespread consensus on how load distribution between the shoulders and pelvis affects the body's metabolic energy expenditure. However, some studies suggested that the partial load transfer used to distribute the load between the upper and lower body has been shown to enhance metabolic energy efficiency [18], [46]–[48].

*Remark 3:* Studies suggest that distributing the load between the shoulders and pelvis during load carriage enhances body stability and balance, thereby reducing the risk of excessive swinging or imbalance [46]. Reducing such tension can prevent hormonal changes that increase heart rate and metabolism, ultimately supporting better metabolic efficiency. These analyses are consistent with the findings in [18], which indicate that a more even distribution of loads across the shoulders and pelvis can further enhance the body's metabolic efficiency during load carriage.

## B. Dynamic Load Reduction

In this paper, dynamic load reduction is accomplished through an LLS-type bio-inspired vibration isolator. Instead of implementing a physical vibration isolator, we present a dynamic model of the LLS-type bio-inspired vibration isolator and generate the desired trajectory for vibration isolation, as shown in Fig. 4.

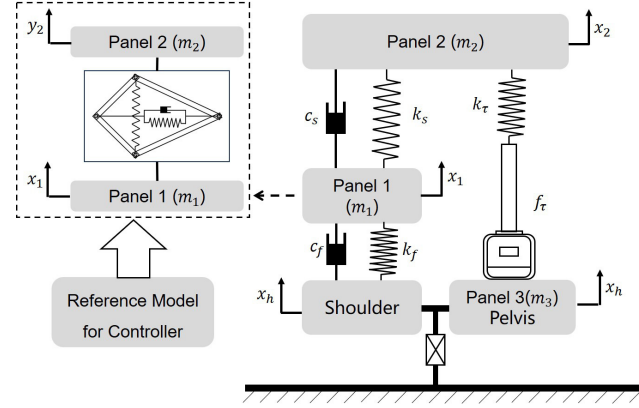


Fig. 4. The suspended backpack with a reference model of the LLS-type bio-inspired vibration isolator.

The LLS-type bio-inspired vibration isolator comprises two rods,  $L_1$  and  $L_2$ , with differing lengths ( $L_2 \geq L_1$ ). The initial angles of these rods, denoted as  $\theta_1$  and  $\theta_2$ , are structured such that  $\theta_1 \geq \theta_2$ , and  $\theta_1 \in (0, \frac{\pi}{2})$ ,  $\theta_2 \in (0, \frac{\pi}{2})$ , as depicted in Fig. 5 (a). A parallel arrangement features a horizontal damping  $c_h$  and a linear spring  $k_h$ , with both components placed between two joints, while a spring with stiffness  $k_v$  in the vertical direction is used. Following the structural deformation,  $\varphi_1$  and  $\varphi_2$  are the variables of angles after the structure deformation, as shown in Fig. 5 (b).  $d_1$  and  $d_2$  are the variable displacements in the horizontal direction.  $x_1$  represents the absolute displacement of panel 1, while  $y_2$  denotes the absolute displacement after passing through the LLS-type bio-inspired vibration isolator. The mass of the isolation object is the load in the backpack system  $m_2$ .

To incorporate this vibration isolation structure into the active load-transfer backpack, a comprehensive modeling approach encompassing geometry, kinematics, and dynamics is employed.

1) *Geometry:* Such a structure conforms to the following geometry, given by:

$$\begin{cases} L_1 \sin(\theta_1) = L_2 \sin(\theta_2), \\ d_i = L_i (\cos(\theta_i) - \cos(\theta_i + \varphi_i)), \\ \tan(\theta_i + \varphi_i) = \frac{L_i \sin(\theta_i) + h}{L_i \cos(\theta_i) - d_i}, \\ \cos(\theta_i + \varphi_i) = \sqrt{1 - \left(\sin(\theta_i) + \frac{h}{L_i}\right)^2}, \quad (i = 1, 2) \\ d_h = d_1 + d_2, \\ \varphi = \varphi_1 + \varphi_2, \\ y = 2h = y_2 - x_1, \\ 0 < \theta_i < \frac{\pi}{2}, \end{cases} \quad (12)$$

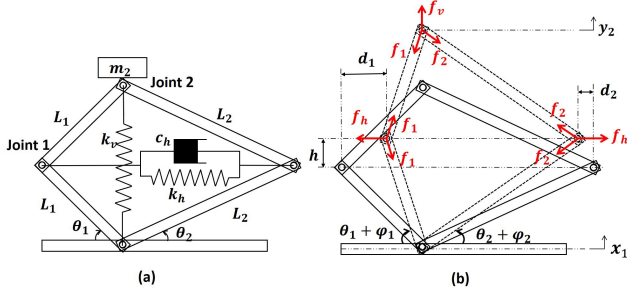


Fig. 5. Schematic view of a bio-inspired vibration isolator.

2) *Statics*: In equilibrium, the vertical and horizontal forces on the three joints are shown in Fig. 5 (b), given by

$$\begin{cases} f_h = k_h d_h = 2f_i \cos(\theta_i + \varphi_i) \\ f_v = \sum_{k=1}^2 f_k \sin(\theta_k + \varphi_k) + 2k_v h \end{cases}, i = 1, 2 \quad (13)$$

Substituting (12) into (13), the dimensionless form of  $f_v$  can be rewritten as:

$$f = \left( \sqrt{1 - \gamma^2} + \sqrt{\beta^2 - \gamma^2} - \sqrt{1 - \psi^2} - \sqrt{\beta^2 - \psi^2} \right) \times \frac{1}{2} \left[ \frac{\psi}{\sqrt{1 - \psi^2}} + \frac{\psi}{\sqrt{\beta^2 - \psi^2}} \right] + 2\alpha\varsigma, \quad (14)$$

$$\psi = \gamma + \varsigma \quad (15)$$

where  $f = \frac{f_v}{k_h L_1}$  is the dimensionless force;  $\beta = \frac{L_2}{L_1}$  is the rod-length ratio;  $\alpha = \frac{k_v}{k_h}$  is the vertical to horizontal spring stiffness ratio;  $\varsigma = \frac{h}{L_1}$  is the dimensionless displacement;  $\gamma = \sin(\theta_1)$  is the initial assembly angle parameter.

From (14), the stiffness of this structure and its derivative in the vertical direction are expressed as:

$$\begin{cases} \frac{\partial f}{\partial \varsigma} = \frac{\partial f}{\partial \psi} \frac{\partial \psi}{\partial \varsigma} = \frac{1}{2} \Psi_1^2 + \frac{1}{2} \Psi_2 \Psi_3 + 2\alpha \\ \frac{\partial^2 f}{\partial \varsigma^2} = \frac{3}{2} \Psi_1 \Psi_3 + \frac{1}{2} \Psi_2 \Psi_4 \end{cases} \quad (16)$$

where  $\Psi_0 = \frac{1}{\sqrt{1 - \psi^2}} + \frac{1}{\sqrt{\beta^2 - \psi^2}}$ ,  $\Psi_1 = \psi \Psi_0$ ,  $\Psi_2 = \frac{1}{\sqrt{1 - \gamma^2}} + \frac{1}{\sqrt{\beta^2 - \gamma^2}} - \frac{1}{\sqrt{1 - \psi^2}} - \frac{1}{\sqrt{\beta^2 - \psi^2}}$ ,  $\Psi_3 = \frac{1}{\sqrt{1 - \psi^2}} + \frac{1}{\sqrt{\beta^2 - \psi^2}} + \frac{\psi^2}{(1 - \psi^2)^{\frac{3}{2}}} + \frac{\psi^2}{(\beta^2 - \psi^2)^{\frac{3}{2}}} = \frac{1}{(1 - \psi^2)^{\frac{3}{2}}} + \frac{\beta^2}{(\beta^2 - \psi^2)^{\frac{3}{2}}}$ ,  $\Psi_4 = \frac{3\psi}{(1 - \psi^2)^{\frac{3}{2}}} + \frac{3\beta^2 \psi}{(\beta^2 - \psi^2)^{\frac{3}{2}}}$ .

The minimum point of the structure stiffness in the vertical direction is calculated by solving  $\frac{d^2 f}{d\varsigma^2} = 0$ . With a solution  $\psi = 0$ , the smallest stiffness is obtained by substituting  $\varsigma = -\gamma$  into (16), given by

$$S_{\min} = \frac{\beta + 1}{2\beta} \left( \sqrt{1 - \gamma^2} + \sqrt{\beta^2 - \gamma^2} - 1 - \beta \right) + 2\alpha \quad (17)$$

where  $S_{\min} > 0$  is to guarantee a positive-only stiffness within the whole working range in the compression. Thus, the extension is from  $(0, \frac{\pi}{2} - \theta_i)$ .

The vertical stiffness of the this bio-inspired vibration isolator is a nonlinear function about the displacement. By

adopting the Taylor expansion for (16) at  $y = 0$ , the vertical stiffness can be rewritten as:

$$f_k(y) = w_0 + w_1 y + \dots + w_n y^n + \dots \quad (18)$$

where  $w_0 = f_k(0)$ ,  $w_1 = \left. \frac{\partial f_k}{\partial y} \right|_{y=0}$ ,  $w_n = \left. \frac{\partial^n f_k}{\partial y^n} \right|_{y=0}$ . The linear stiffness  $w_0$  is a dominant factor to resonant frequency of this isolator at  $y = 0$  which is a function of the parameters  $\alpha, \beta, \gamma$ , given by

$$w_0 = \frac{\gamma^2}{2} \left( \frac{1}{\sqrt{1 - \gamma^2}} + \frac{1}{\sqrt{\beta - \gamma^2}} \right)^2 + 2\alpha \quad (19)$$

The resonant frequency should be designed to be low to meet the vibration isolation requirements.

3) *Dynamics*: The dynamics of such a structure is built by using the Lagrange principle. The kinetic energy is given by:

$$T = \frac{1}{2} m_2 \dot{y}_2^2 \quad (20)$$

The system starts to move from the equilibrium point ( $k_v \Delta y = m_2 g$ ) and the potential energy  $U$  can be expressed as:

$$U = \frac{1}{2} k_h d_h^2 + \frac{1}{2} k_v (y - \Delta y)^2 + m_2 g y_2 \quad (21)$$

The dynamics of the vibration isolator is calculated by using Lagrangian equation:

$$\frac{\partial}{\partial t} \left( \frac{\partial L}{\partial \dot{y}_2} \right) - \frac{\partial L}{\partial y_2} = -c_1 \dot{y} - c_h \dot{d}_h \frac{\partial d_h}{\partial y_2} - c_3 n_x \dot{\varphi} \frac{\partial \varphi}{\partial y_2} \quad (22)$$

where  $L = T - U$ .  $n_x$  is the number of joints.  $c_1$ ,  $c_h$  and  $c_3$  are the air damping, the horizontal damping and the rotational friction coefficient of each joint, respectively. The dynamics is written as:

$$m_2 \ddot{y} + \left[ c_1 + c_h \left( \frac{\partial d_h}{\partial y} \right)^2 + c_3 n_x \left( \frac{\partial \varphi}{\partial y} \right)^2 \right] \dot{y} + k_v y + k_h d_h \frac{\partial d_h}{\partial y} = -m_2 \ddot{x}_1 \quad (23)$$

According to (12), we have

$$\frac{\partial d_h}{\partial y} = \frac{\psi}{2\sqrt{1 - \psi^2}} + \frac{\psi}{2\sqrt{\beta^2 - \psi^2}} = \frac{1}{2} \Psi_1 \quad (24)$$

$$\frac{\partial \varphi}{\partial y} = \frac{1}{2L_1} \left( \frac{1}{\sqrt{1 - \psi^2}} + \frac{1}{\sqrt{\beta^2 - \psi^2}} \right) = \frac{\Psi_0}{2L_1} \quad (25)$$

Let the excitation  $-\ddot{x}_1$  be the system input  $U$ ,  $U = -\ddot{x}_1$ . The system (23) can be rewritten as:

$$\begin{cases} \dot{Y}_1 = Y_2 \\ \dot{Y}_2 = -\frac{1}{m_2} \left( c_1 + \frac{c_h}{4} \Psi_1^2 + \frac{c_3 n_x}{4L_1^2} \Psi_0^2 \right) Y_2 \\ \quad - \frac{k_v}{m_2} Y_1 - \frac{k_h d_h}{2m_2} \Psi_1 + U \\ Y = Y_1 = y \end{cases} \quad (26)$$

To ensure the overall stability of the system, we must verify that the vibration isolator's output remains bounded under bounded excitations, which essentially reflects the concept of input-output stability.

*Lemma 1:* Given that the LLS-type bio-inspired vibration isolator (26) works within the range of the positive-only stiffness, the system exhibits  $L_\infty$  stable from  $(U, Y)$ . See Appendix A.

*Remark 4:* For the Lemma 1, the key distinction between this paper and [28] lies in the perspective taken: [28] proves ultimate uniform boundedness, whereas this paper proves input-output stability. While both input-output stability and ultimate uniform boundedness are related to system stability, they describe different aspects. Specially, input-output stability assesses how a system's output responds to bounded inputs, ensuring that the output remains bounded if the input is bounded, without specific requirements on the long-term behavior of the system state. In contrast, ultimate uniform boundedness emphasizes the system's long-term behavior, guaranteeing that the system state will eventually remain within a bounded region as time progresses toward infinity. For the application of vibration isolators, input-output stability is more direct, as it ensures the system's real-time responses to excitations, rather than long-term stability assurance.

Consequently, when the motion of the load  $x_\rho$  follows the same motion pattern as  $y$ , it effectively emulates the functionality of the LLS-type bio-inspired vibration isolator.

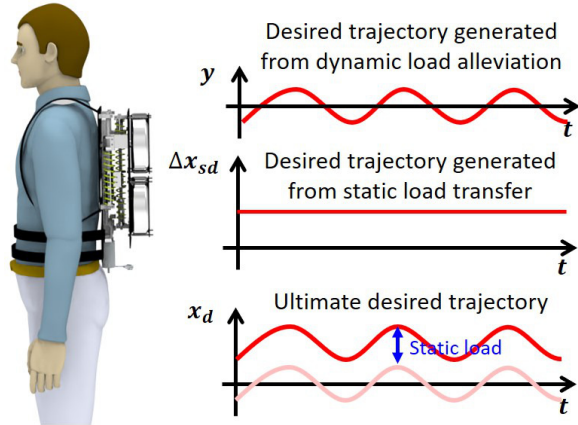


Fig. 6. Desired trajectory incorporating dynamic load reduction and static load transfer.

Lastly, leveraging the insights gained from the prior analyses of section III.A and III.B, we can formulate a unified desired trajectory  $x_d = y + \Delta x_{sd}$ . As the load's motion follows this reference trajectory, it brings about the simultaneous realization of both static load transfer and dynamic load alleviation.

*Remark 5:* Load transfer is realized by establishing a desired load transfer ratio  $\xi_d$ , which determines the desired position  $\Delta x_{sd}$  through the principle of system force equilibrium. Since  $\xi_d$  remains constant,  $\Delta x_{sd}$  is also fixed, essentially adjusting only the equilibrium position of the load  $m_2$ . These two desired trajectories  $\Delta x_{sd}$  and  $y$  operate independently of each other and have no mutual influence, as  $\Delta x_{sd}$  neither affects  $\ddot{x}_1$  and  $\ddot{x}_2$ , nor changes the variation pattern of  $y$ , as shown in Fig. 6. This allows the SEA-based controller to ensure that  $x_\rho$  effectively follows  $x_d = y + \Delta x_{sd}$ , achieving both static load transfer and dynamic load reduction.

## IV. CONTROLLER DESIGN

This section proposes an SEA-based controller with prescribed performance to achieve tracking tasks while ensuring the load operates in the range. The control scheme is shown in Fig. 7.

### A. Constraint System Transformation

In this part, we employ prescribed performance functions to build the load's motion constraints. The tracking error  $e(t) = x_\rho - x_d$  is defined where  $x_d$ ,  $\dot{x}_d$ , and  $\ddot{x}_d$  are continuously differentiable and bounded by  $x_m$  according to Lemma 1. The constraint is built if  $e(t)$  fulfills the following condition:

$$\underline{\delta}(t) < e(t) < \bar{\delta}(t) \quad (27)$$

where  $\bar{\delta}(t)$  and  $\underline{\delta}(t)$  are respectively the upper and lower bounds computed by a positive constant  $\mu$  and a decreasing smooth prescribed function  $\rho(t) = (\rho_0 - \rho_\infty)e^{-kt} + \rho_\infty$  with  $\rho_0 > \rho_\infty > 0$  and  $k > 0$ , given by

$$\bar{\delta}(t) = \mu\rho(t), \underline{\delta}(t) = -\mu\rho(t). \quad (28)$$

The constraint problem is converted into an equivalent unconstrained one by using a transformation function:

$$-\mu \leq \zeta(z) \leq \mu, \zeta(z) = \mu \frac{e^z - e^{-z}}{e^z + e^{-z}} \quad (29)$$

The equivalent form (27) is  $e(t) = \rho(t)\zeta(z)$ , and the unconstrained tracking error is denoted as:

$$z = \frac{1}{2} \ln \frac{e - \delta}{\delta - e} = \frac{1}{2} \ln \frac{\delta + e}{\delta - e} \quad (30)$$

where  $\delta = \bar{\delta} = -\underline{\delta}$ . It follows that

$$\dot{z} = \frac{1}{\vartheta_1} \dot{e} - \frac{1}{\vartheta_2} \dot{\delta}, \quad (31)$$

$$\dot{e} = \vartheta_1 \dot{z} - \delta_e^*, \quad (32)$$

$$\ddot{e} = \vartheta_1 \ddot{z} + \dot{\vartheta}_1 \dot{z} - \delta_e^*, \quad (33)$$

where  $0 < \vartheta_1 = \delta - \frac{e^2}{\delta} < 1$ ,  $\vartheta_2 = \frac{\delta^2}{e} - e$ ,  $\delta_e^* = \delta^* e$ ,  $\delta^* = -\frac{\dot{\delta}}{\delta}$ . Substituting (31) and (33) into (6), the dynamics of the backpack is rewritten as:

$$M_z \ddot{z} + C_z \dot{z} + G_z + \vartheta_1 k_\tau (x_{h2} - l_b \theta) = \vartheta_1 f_\rho + \vartheta_1 \nu_\rho \quad (34)$$

where  $M_z = m_2 \vartheta_1^2$ ,  $C_z = m_2 \vartheta_1 \dot{\vartheta}_1 + c_\rho \vartheta_1^2$ , and  $G_z = \vartheta_1 (k_\rho x_\rho + m_2 (\ddot{x}_d - \delta_e^*) + c_\rho (\dot{x}_d - \delta_e^*))$

With the definition of a sliding manifold  $\sigma_z = \dot{z} + \lambda_z z$ , (34) can be rewritten as:

$$M_z \dot{\sigma}_z + C_z \sigma_z + \vartheta_1 k_\tau x_{h2} = \vartheta_1 f_\rho + \vartheta_1 \nu_\rho + \vartheta_1 k_\tau l_b \theta + M_z \lambda_z \dot{z} + C_z \lambda_z z - G_z \quad (35)$$

where  $\lambda_z$  is a positive constant.

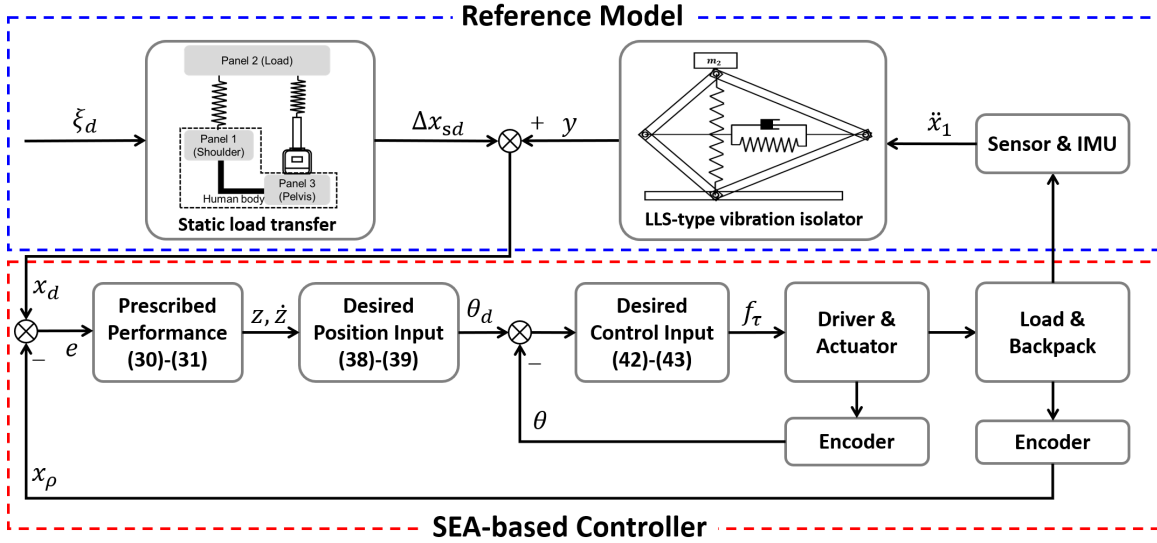


Fig. 7. Control framework for the active load-transfer backpack.

### B. SEA-based Controller with Prescribed Performance

The controller is generated based on a sliding manifold,

$$\sigma_x = \dot{x}_\rho - \dot{x}_r = \dot{x}_\rho - (\dot{x}_\rho - \vartheta_1 \sigma_z) \quad (36)$$

where  $\dot{x}_r = \dot{x}_\rho - \vartheta_1 \sigma_z$  is a velocity reference. Thus, substituting (36) into (6), the dynamics can be written as:

$$m_2 \dot{\sigma}_x + c_\rho \sigma_x + \Lambda(x_\rho, \dot{x}_r, \ddot{x}_r)^T \phi_x + k_\tau (x_{h2} - l_b \theta_d) = f_\tau + \nu_\rho + k_\tau l_b \Delta \theta \quad (37)$$

where  $\Delta \theta = \theta - \theta_d$ ;  $\Lambda(x_\rho, \dot{x}_r, \ddot{x}_r) = [x_\rho, \dot{x}_r, \ddot{x}_r]^T$  and  $\phi_x = [k_\rho, c_\rho, m_2]^T$ . Thus, the virtual motor position is regarded as a virtual control signal for the system dynamics, given by

$$\theta_d = \frac{1}{l_b} \left( x_{h2} - \frac{1}{k_\tau} \left( \kappa_x \sigma_x - \Lambda(x_\rho, \dot{x}_r, \ddot{x}_r)^T \hat{\phi}_x \right) \right) \quad (38)$$

where  $\kappa_x$  is a positive constant.  $\hat{\phi}_x$  is the estimation of  $\phi_x$  whose adaption law is expressed as:

$$\dot{\hat{\phi}}_x = -\sigma_x \Gamma_x \Lambda(x_\rho, \dot{x}_r, \ddot{x}_r) \quad (39)$$

where  $\Gamma_x = \text{diag}\{\Gamma_{x1}, \Gamma_{x2}, \Gamma_{x3}\} \in \mathfrak{R}^{3 \times 3}$  is a positive definite matrix.  $\phi_x = \phi_x - \hat{\phi}_x$  and  $\|\phi_x\| < \phi_m$ .

In the subsequent, the control input for the motor actuation  $\tau$  is proposed to allow  $\theta$  to track the desired input  $\theta_d$ . Another sliding manifold is defined as

$$\sigma_\theta = \dot{\theta} - \dot{\theta}_r = \Delta \dot{\theta} + \lambda_\theta \Delta \theta \quad (40)$$

where  $\lambda_\theta$  is a positive constant and  $\dot{\theta}_r = \dot{\theta}_d - \lambda_\theta (\theta - \theta_d)$ . Hence, the dynamics of the actuator can be rewritten as:

$$J \dot{\sigma}_\theta + b \sigma_\theta + \Lambda(\dot{\theta}_r, \ddot{\theta}_r)^T \phi_\theta + k_\tau (l_b \theta - x_{h2}) = f_\tau + \nu_\tau \quad (41)$$

where  $\Lambda(\dot{\theta}_r, \ddot{\theta}_r) = [\dot{\theta}_r, \ddot{\theta}_r]^T$  and  $\phi_\theta = [b, J]^T$ . The control input of the system is described as:

$$f_\tau = -\kappa_\theta \sigma_\theta + k_\tau (l_b \theta - x_{h2}) + \Lambda(\dot{\theta}_r, \ddot{\theta}_r)^T \hat{\phi}_\theta \quad (42)$$

where  $\kappa_\theta = \kappa_{\theta 1} + \kappa_{\theta 2}$ .  $\kappa_{\theta 1}$  and  $\kappa_{\theta 2}$  are positive constants.  $\hat{\phi}_\theta$  is the estimation of  $\phi_\theta$  with the adaption law:

$$\dot{\hat{\phi}}_\theta = -\Gamma_\theta \sigma_\theta \Lambda(\dot{\theta}_r, \ddot{\theta}_r) \quad (43)$$

where  $\Gamma_\theta$  is a positive constant and  $\tilde{\phi}_\theta = \phi_\theta - \hat{\phi}_\theta$ .

*Theorem 1:* The closed-loop system (37)-(43) exhibits the passivity of the dynamics between the input  $f_\rho$  and the output  $\sigma_x$ , if the disturbances terms  $\nu_\rho = 0, \nu_\tau = 0$  and the parameters are chosen such that

$$(c_\rho + \kappa_x - \frac{1}{2}) \kappa_{\theta 2} \lambda_\theta^2 > \frac{1}{4} k_\tau^2 l_b^2 \quad (44)$$

See Appendix B.

*Theorem 2:* For the system (6) and (7) with the initial condition  $\delta(0) < e(0) < \bar{\delta}(0)$ , the controller (38), (39), (42) and (43) preserves the position constraints (27) if  $f_\rho$  is bounded by a positive constant  $f_m$ , the disturbance  $\nu_\rho$  is bounded by  $\bar{\nu}_\rho$ , the disturbance  $\nu_\tau$  is bounded by  $\bar{\nu}_\tau$ , and the following parameters are chosen such that  $\kappa_{\theta 1} + b > \frac{1}{4}$ . See Appendix C.

## V. SIMULATION ANALYSIS

The human-backpack system was implemented by identifying the parameters, which were presented in Table I.

TABLE I  
THE PARAMETERS OF THE BACKPACK SYSTEM.

	Value		Value
$k_s$	1540(N/m)	$c_s$	43.9(N · s/m)
$J_m$	$5.38 \times 10^{-6}(kg \cdot m^2)$	$b_m$	$4.22 \times 10^{-5}(N \cdot m/rad)$
$k_\tau$	2910(N/m)	$k_u$	0.0232(N · m/A)
$m_1$	1.4(kg)	$m_2$	variable
$l_b$	$7.96 \times 10^{-4}(m/rad)$	$m_3$	1.75(kg)

This paper used three typical application scenarios to verify the effectiveness of the algorithm, including walking on level ground, ascending stairs, and walking on a complex terrain.

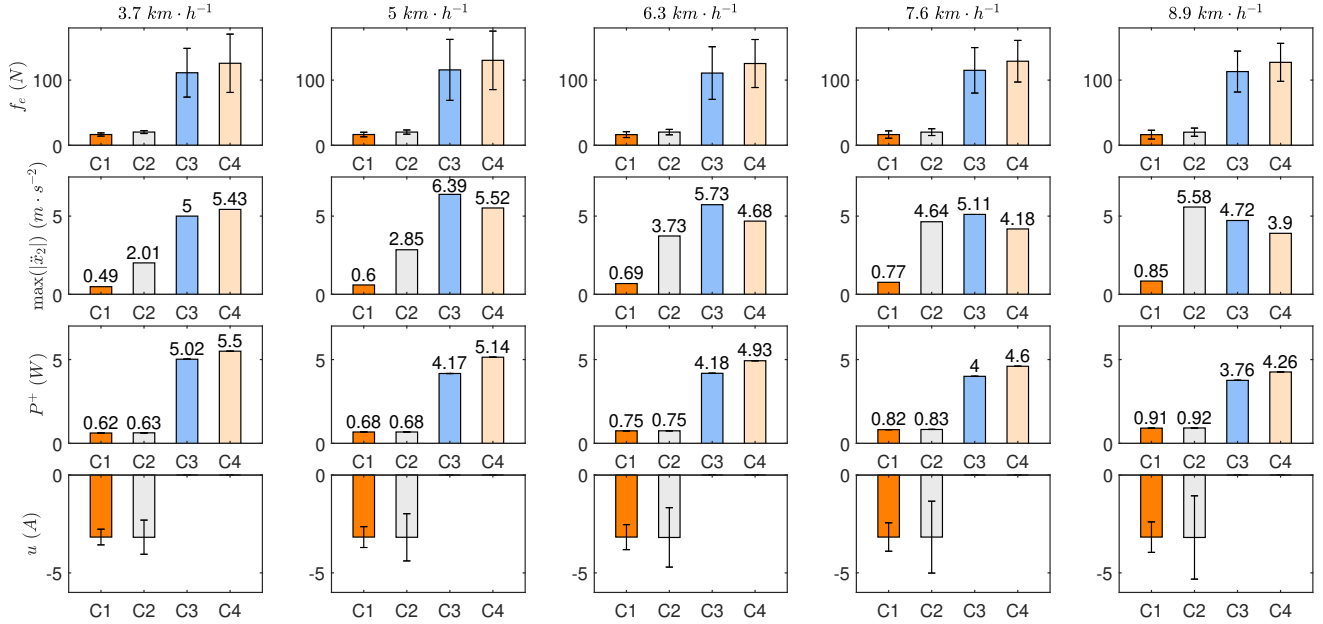


Fig. 8. System performance when a subject walked on level-ground. The first row shows the shoulder pressure in C1, C2, C3 and C4 where the bar stands for the bias value and the error bar denotes the amplitude; the second row represents the maximum absolute value of the vertical acceleration of the load; the third row exhibits the net mechanical work done by the interaction force; the fourth row is the bias and amplitude of the controller output.

The parameters of the proposed method were chosen as:  $k_x = 20.5, k_\theta = 1.5, \lambda_z = 50, \lambda_\theta = 0.5$ . The parameters of the LLS-type bio-inspired vibration isolator should meet the condition (17) to guarantee a positive-only stiffness. The parameters were chosen as:  $L_1 = 0.05(m), L_2 = 0.1(m), \theta_1 = \pi/6(rad), \theta_2 = 0(rad), k_h = 200(N/m), k_v = 15(N/m), c_1 = 0.1(N \cdot s/m), c_h = 1000(N \cdot s/m), c_3 = 1.5(N \cdot s/m)$ . The human-robot interaction force  $f_e$  was supposed to be a spring between  $x_1$  and  $x_h$  with  $k_f = 5060(N/m)$  and  $c_f = 320(N \cdot s/m)$ .

To demonstrate the proposed method, the following cases were depicted for comparisons:

- Case 1 (C1): The active backpack system was controlled by the proposed method in this paper.
- Case 2 (C2): The active backpack system was controlled by an impedance control method based on human-robot interaction force proposed in our previous work [16];
- Case 3 (C3): The control circuit was powered off and the system took on the form of a passive backpack without actuation component;
- Case4 (C4): The system took on the form of a passive backpack with actuation component;

Obviously, after removing the actuation components, the system presented in this paper is necessarily a passive suspended backpack with unchanged springs. Compared to C4, the main difference in C3 is that panel 3 is reduced by 1.63 kg, and panel 2 is reduced by 1.53 kg.

As direct measurement of the human body's metabolic energy is not feasible in the simulation validation, we address the energy benefit from the backpack by considering mechanical energy. Hence, we introduce the RMS value of positive

mechanical energy, defined as:

$$P^+ = \sqrt{\frac{1}{T} \int_0^T P_f^+(t)^2 d\zeta}, \quad P_f^+(t) = \begin{cases} f_e \dot{x}_\sigma, f_e \dot{x}_\sigma > 0 \\ 0, & \text{others} \end{cases} \quad (45)$$

where  $P_f^+(t)$  denotes the positive power of  $f_e$ .

#### A. Walking on Level Ground

The vertical motion of the human center of mass during locomotion was approximated as a sinusoid characterized by a constant amplitude and frequency. The vertical displacement of human COG can be expressed as presented in [11]:

$$x_h(t) = A \sin(\omega_f t) \quad (46)$$

where  $A = 0.02$  (m) is the leg actuator oscillation amplitude. The frequency  $\omega_f$  ( $rad \cdot s^{-1}$ ) was approximated as a function of the walking speed  $v$  ( $km \cdot h^{-1}$ ) and height  $S = 1.8$  (m), given by:

$$\omega_f = \frac{4\pi \times 64.8 [v / (3.6 \times S)]^{0.57}}{60} \quad (47)$$

The subject was assumed to walk at velocities of  $v = \{3.7, 5, 6.3, 7.6, 8.9\}$  ( $km \cdot h^{-1}$ ), while carrying a load mass of 10 kg, to align with the typical walking speed of a healthy individual on level terrain.

The findings are presented in Fig. 8, showing the evolution of the four metrics from left to right to give a more global picture of the suspended backpack's performance. These metrics include human-robot interaction force  $f_e$  at shoulder level, net mechanical work  $P^+$ , load PA  $\max(|\ddot{x}_2|)$ , and motor current  $u$ . Evidently, the following outcomes emerge:

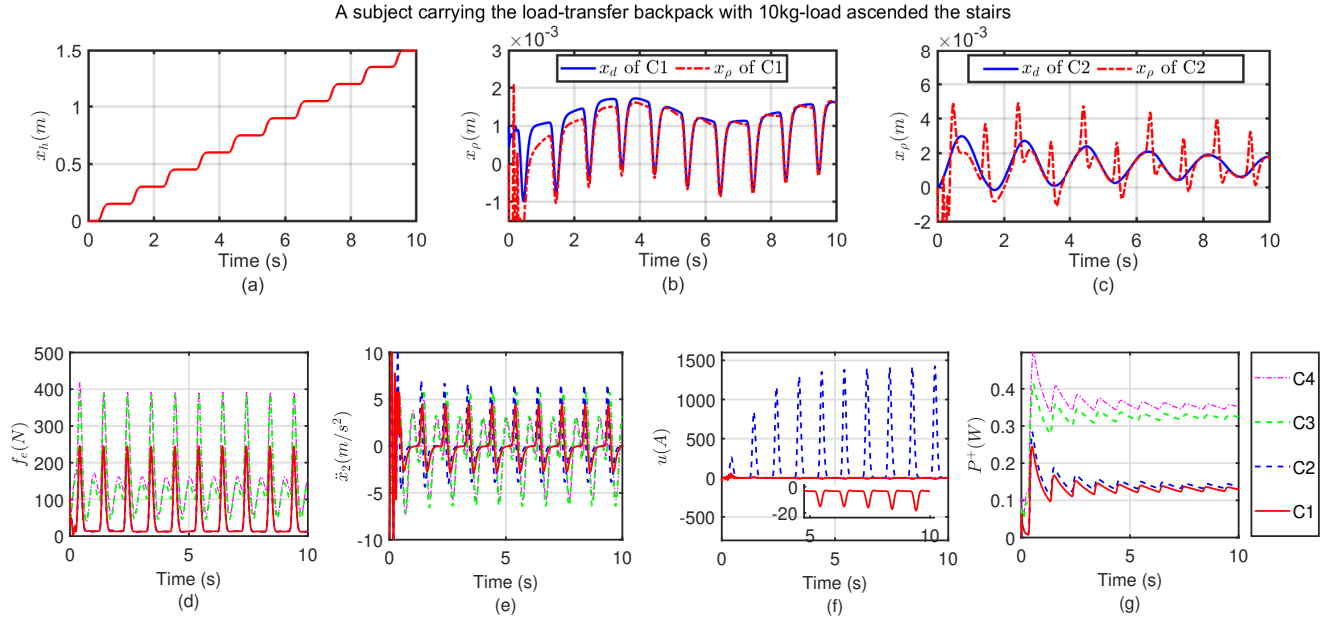


Fig. 9. System performance when a subject walked on stairs. (a) Human vertical motion of the center of mass. (b) Tracking performance of C1. (c) Tracking performance of C2. (d) Human shoulder pressure. (e) Load acceleration. (f) Motor current. (g) Net mechanical power from  $f_e$ .

Compared to the passive case (C4), the active configurations (C1 and C2) demonstrate substantial reductions in bias (C1: 85.13% decrease, C2: 81.87% decrease) and amplitude (C1: 93.35% decrease, C2: 93.95% decrease) of  $f_e$ . This phenomenon persisted even when there was a significant variation in human locomotion speed. This outcome stems from the design of separated panels, enabling the load transfer from the shoulders to the pelvis through motor actuation. Additionally, due to the lack of actuation components, C3 remains a passive suspended backpack without load transfer capability. This results in higher shoulder interaction forces compared to the active configurations (C1 and C2), but still lower than those in C4. This is intuitive because a decrease in the system's mass leads to a reduction in shoulder pressure.

When analyzing the load PA, a conspicuous variation emerged as human motion accelerated. As human movement speed increases, the load's PA in C2 shows a consistent rise, ranging from  $2.01 \text{ m} \cdot \text{s}^{-2}$  to  $5.58 \text{ m} \cdot \text{s}^{-2}$ . In C4, the load's PA exhibited an ascent followed by a descent, peaking at  $6.39 \text{ m} \cdot \text{s}^{-2}$ . Conversely, the load acceleration of C1 registers a moderate increase, spanning from  $0.49 \text{ m} \cdot \text{s}^{-2}$  to  $0.85 \text{ m} \cdot \text{s}^{-2}$ . This observation implies that the LLS-type bio-inspired vibration isolators demonstrate superior adaptability to variations in vibration frequency compared to their linear counterparts. Except at the low speed of  $3.7 \text{ km} \cdot \text{h}^{-1}$  where the vibration of C3 is smaller than that of C4, at subsequent walking speeds of  $5 \text{ km} \cdot \text{h}^{-1}$  to  $8.9 \text{ km} \cdot \text{h}^{-1}$ , the load vibration of C3 is greater than that of C4. This is because the reduced load mass in C3 leads to an increased resonance frequency  $w_d = \sqrt{\frac{k_s}{m_2}}$ .

In terms of  $P^+$ , C1 and C2 exhibited reductions of 88.72% and 88.54%, respectively, in comparison to the value observed in C4, with a subject moving at a speed of  $3.7 \text{ km} \cdot \text{h}^{-1}$ . As

the subject's velocity increases,  $P^+$  tends to increase in all cases. This phenomenon is unsurprising, given that the peak value of  $f_e$  increases with higher stepping frequency. While the lighter C3 exhibits lower  $P^+$  compared with C4, because for the passive suspended backpacks, the load mass is clearly the main factor affecting mechanical energy.

For the system input, C1 exhibited a similar motor current bias to C2, and this characteristic remains consistent regardless of the speed of human motion. However, the amplitude of the current tends to increase as the speed of the human body rises, with C1's amplitude change being considerably smaller than that of C2. Specifically, when comparing the speed at  $3.7 \text{ km} \cdot \text{h}^{-1}$  with that at  $8.9 \text{ km} \cdot \text{h}^{-1}$ , the amplitudes of C1 and C2 increase by 94.4% and 143.91%, respectively. Notably, even at the highest speed, C1's amplitude remains lower than C2's amplitude at the lowest speed. These observations imply that C1 demonstrates superior energy efficiency across various operation speeds.

### B. Ascending Stairs

In this section, we consider a scenario where the subject is ascending a set of stairs. Each individual step's height is fixed at 15 cm, and the subject takes 1.0 second to ascend from one step to the next. Consequently, the change in vertical motion of the human COG per step can be mathematically described as follows:

$$x_h(t) = x_{h0} \left[ \left( \frac{t^2 - t_1^2}{t_1^2 - t_0^2} \right)^{16} - 1 \right], t_0 \leq t < t_1 \quad (48)$$

where  $x_{h0} = 15 \text{ cm}$  is the height of each stair and  $t_1 - t_0 = 1$  second is the time for the subject to ascend each step. Thus, over a period of time, the vertical motion of the human centre of mass is shown in Fig. 9(a).

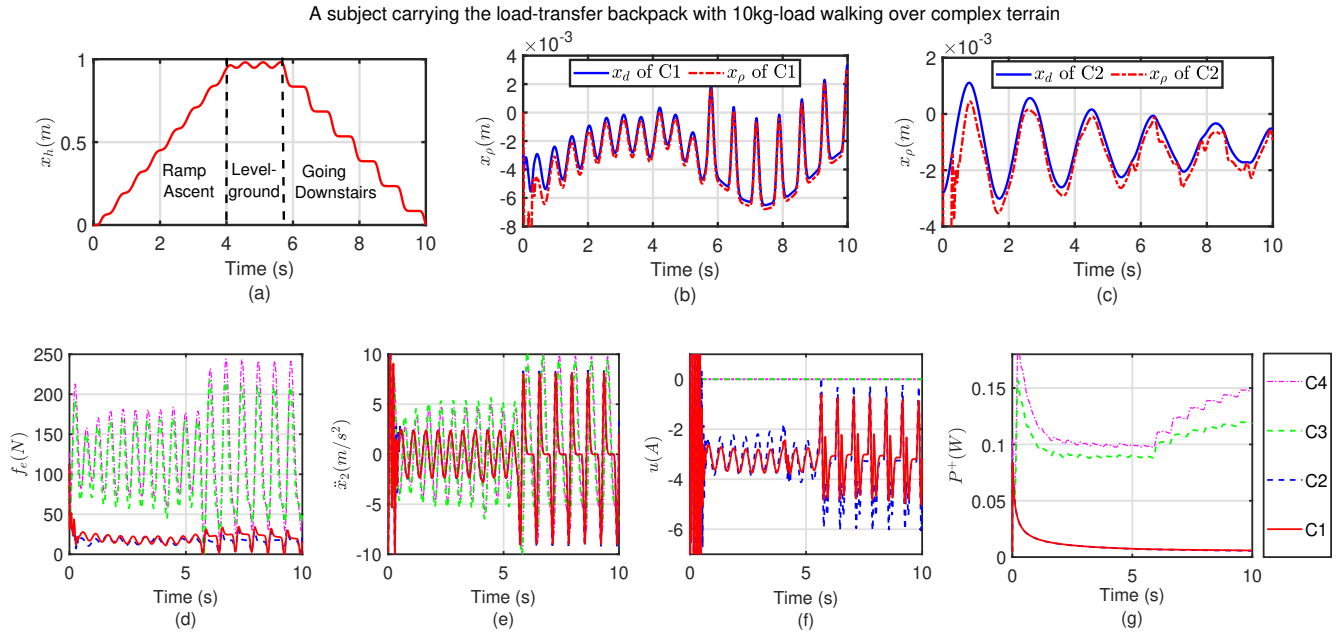


Fig. 10. System performance when a subject walked over complex terrain. (a) Human vertical motion of the center of mass. (b) Tracking performance of C1. (c) Tracking performance of C2. (d) Human shoulder pressure. (e) Load acceleration. (f) Motor current. (g) Net mechanical power from  $f_e$ .

Analyzing Fig. 9(b) and Fig. 9(c), it is evident that, unlike the previous case, the reference trajectories generated by C1 and C2 exhibit complete dissimilarity. This difference stems from C1 as a nonlinear vibration isolator, in contrast to C2, which functions as a linear vibration isolator. This leads to distinct tracking behaviors by the controller, even when the controller's parameters are kept unchanged. Subsequent analysis of performance indicators (depicted in Fig. 9(d) to Fig. 9(g)) reveals that, while C1 and C2 yield similar outcomes in terms of  $f_e$ ,  $\ddot{x}_2$ , and  $P^+$ , a significant deviation arises in the input current of C2, surpassing the system's capacity. When comparing the C3 and C4 cases, since both are passive suspended backpacks, the peaks of shoulder pressure, the levels of shoulder pressure and vibration amplitude are comparable. Due to the slightly larger load of C4, its  $P^+$  is greater than that of C3.

This difference implies that the linear vibration isolator (C2) might not be suitable for intricate application scenarios like ascending stairs. Conversely, the LLS-type bio-inspired vibration isolator proves more adept at generating references trajectories that align closely with human motion patterns.

### C. Walking on Complex Terrain

In this section, we examine a challenging terrain featuring slopes, level ground, and stairs. The subject initially ascends a 10-degree slope, followed by walking on a flat ground, and concluding with a descent down a flight of stairs. In this instance, we can simplify the modeling of the vertical motion

of the human center of mass with the following function:

$$x_h(t) = \begin{cases} A \sin(w_f t) + \frac{v}{3.6} \sin(\frac{\pi}{18})t, & t \in [0, t_0) \\ A \sin(w_f t) + \frac{v}{3.6} \sin(\frac{\pi}{18})t_0, & t \in [t_0, t_1) \\ 1 - x_{h0} \left[ \left( \frac{t^2 - t_u^2}{t_u^2 - t_s^2} \right)^{16} - 1 \right], & t \in [t_s, t_u) \end{cases} \quad (49)$$

where  $t_s \geq t_1$ .  $t_u - t_s$  represents the duration required for a single step in walking, similar to the previous section of ascending stairs.

The function curve is depicted in Fig. 10(a). During the first 4 seconds ( $t_0 = 4$ ),  $x_h$  exhibits behavior resembling a combination of a smoothly changing bias and a constant-frequency sinusoidal component, signifying the subject's uphill movement on a 10-degree slope. Subsequently, over the next 1.8 seconds, from  $t_0$  to  $t_1$ ,  $x_h$  follows a sinusoidal pattern with a fixed bias, representing the subject's movement on level ground. In the ensuing 4.2 seconds,  $x_h$  experiences periodic descent, corresponding to the subject's descent of a staircase. Notably, similar to the previous stair ascent, each step maintains a consistent height of  $x_{h0} = 15$  cm, with a time interval of  $t_u - t_s = 0.7$  seconds.

In Fig. 10(b), it is evident that C1 generates comparable trajectories while walking uphill and on flat ground, but displays noticeably distinct trajectories when descending stairs. This indicates that the proposed bio-inspired vibration isolator is capable of producing varying results in response to changes in terrain. In contrast, as shown in Fig. 10(c), C2 consistently generates similar curves across different terrains, highlighting the constrained capacity of the linear vibration isolator to adapt to varying terrains.

Regarding the indices presented in Fig. 10(d)-Fig. 10(g), the decline in  $f_e$  and PA remains significantly pronounced in

C1 and C2 in comparison to C4, and there is a significant reduction in net mechanical power, indicating that the active case effectively regulates load movement. When comparing C1 and C2, despite their disparate trajectories, both demonstrate comparable performance in terms of  $f_e$ , PA, and mechanical energy. This can be attributed to the nearly unlimited bandwidth and high sampling frequencies in the simulation, but C1 produces a lower peak current compared to C2, underscoring the superior energy efficiency of the proposed approach. When comparing C3 and C4, We can draw similar conclusions to those observed in the ascending stairs scenario. Due to the smaller load mass in C3, shoulder pressure in C3 is relatively lower, while the corresponding vibration levels remain similar and  $P^+$  is higher.

## VI. EXPERIMENTAL VALIDATION

The total weight of the backpack is 4.5 kg, including carbon fiber panels, various accessories, and an active module, as depicted in Fig. 11. Main components within the active module include a brushless DC motor (EC 40 170W, Maxon, Swiss) equipped with an encoder, a motor driver (EPOS4 Compact 50/15 CAN, Maxon, Swiss), an air pressure sensor (XGZP6847A, CFSensor, China) utilized to estimate interaction forces exerted on the shoulder, optical encoders (E6B2-CWZ3E, OMRON, USA) responsible for measuring the relative displacement of the panels, as well as a battery unit. Additionally, the setup integrates two IMUs (LPMS-B2, LP-Research Inc., Japan) to capture the vertical accelerations of both the carrier and the load. The supplementary accessories consist of a ball screw (LX2005P-B1-N-300, MISUMI, Japan) and springs (SWY30, MISUMI, Japan) integrated into the Swing Backpack System (SBS) and Swing Support Structure (SS) respectively. A Raspberry Pi 4 Model B ensures the implementation of closed-loop control. This system established communication with the motor driver through the CANopen protocol, while utilizing GPIOs to obtain digital signals from the encoder.

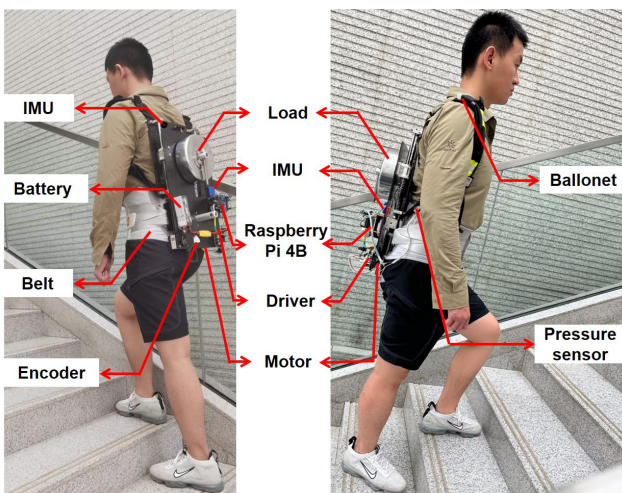


Fig. 11. Schematic view of human load carriage through the backpack.

### A. Experimental Protocol

Eight healthy volunteers participated in the experiments. Prior to the experiments, all subjects were thoroughly in-

TABLE II  
PARTICIPANTS' PERSONAL INFORMATION

Subject	Gender	Age	Height	Weight
S1	male	25	181 (cm)	70 (kg)
S2	male	22	183 (cm)	90 (kg)
S3	male	22	168 (cm)	71 (kg)
S4	male	28	168 (cm)	64 (kg)
S5	male	26	173 (cm)	63 (kg)
S6	male	27	177 (cm)	70 (kg)
S7	male	25	164 (cm)	80 (kg)
S8	male	33	167 (cm)	61 (kg)

formed about the experimental protocols, and their written consent was obtained. The participants' personal information is presented in Table II. The protocol was approved by local board from the Ethics Committee of Tongji Medical College, Huazhong University of Science and Technology (IORG No: IORG0003571). Necessary precautions were taken to ensure the safety of participants, along with safeguarding the privacy and confidentiality of their personal information.

Participants were requested to carry the backpack with 10kg-load and engaged in experimental trials on a treadmill, a staircase and a complex terrain including ramps, stairs, and level-ground. The experiments were designed to include four distinct conditions for each terrain type:

- 1) LOCKED: The load was locked to the panel 1 and the actuation module was power off;
- 2) PASSIVE: The load was not locked and the actuation module was power off;
- 3) ACTIVE-IROS: The backpack was controlled by an impedance controller presented in our previous work [16].
- 4) ACTIVE-LLS: The backpack was operated with the proposed method.

The difference between PASSIVE and active configurations (including ACTIVE-LLS and ACTIVE-IROS) is that the PASSIVE configuration operates without a power supply, with the equilibrium point determined by the spring stiffness  $k_s$  and the load weight  $m_2$ . To ensure fairness in experimental comparisons, all the configurations used the same springs. Regarding the ACTIVE-IROS case, we set the expected load transfer ratio  $\xi_d = 0.5$  which is the same as the ACTIVE-LLS case. This enables a direct comparison between the IROS [16] method and the LLS-type bio-inspired vibration isolator.

Detailed explanations regarding the experimental setup, procedural methodology, designated rest intervals, and other pertinent information for each specific case will be elaborated upon in the subsequent sections of the experimental description. To compute the net metabolic rate, the data was acquired from a wearable metabolic system (K5, COSMED, Italy), and the metabolic rate during 1-min quiet standing was subtracted from the metabolic rate during loaded walking. This resultant value was then normalized by the respective body mass of each participant. The metabolic reduction is mainly for the ACTIVE-LLS case compared to the LOCKED case. Mean values and their corresponding standard deviations

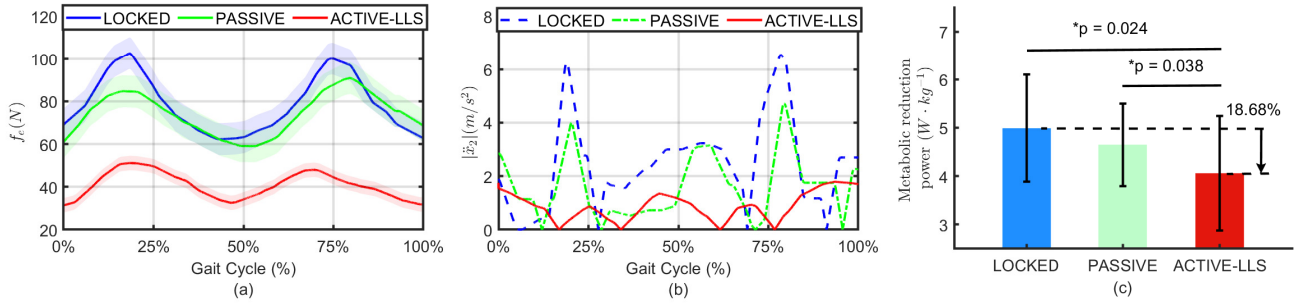


Fig. 12. System performance during human walking on level ground. (a) Shoulder pressure. (b) Vertical load acceleration. (c) Gross metabolic reduction.

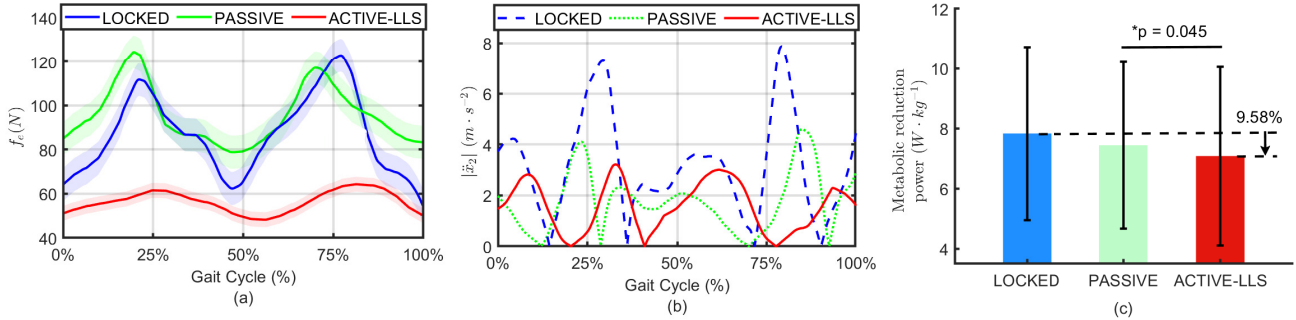


Fig. 13. System performance during human stair ascension. (a) Shoulder pressure. (b) Vertical load acceleration. (c) Gross metabolic reduction.

TABLE III  
PERFORMANCE EVALUATION WITH THE LOAD-TRANSFER BACKPACK

Condition	Index	Walking on Treadmill			Ascending Stairs		
		$f_e$ (N)	MAX( $\ddot{x}_2$ ) ( $m \cdot s^{-2}$ )	Metabolic Reduction ( $W \cdot kg^{-1}$ )	$f_e$ (N)	MAX( $\ddot{x}_2$ ) ( $m \cdot s^{-2}$ )	Metabolic Reduction ( $W \cdot kg^{-1}$ )
LOCKED		80.48 ± 20.18	6.57	4.99 ± 1.11	101.62 ± 22.81	7.87	7.83 ± 2.89
PASSIVE		74.98 ± 15.92	4.71	4.64 ± 0.85	88.57 ± 34.26	4.60	7.44 ± 2.77
ACTIVE-LLS		43.87 ± 9.87	1.79	4.06 ± 1.18	56.26 ± 8.01	3.50	7.08 ± 2.97

TABLE IV  
COMPARATIVE EVALUATION WITH EXISTING CONTROL STRATEGIES DURING HUMAN WALKING ON TREADMILL

	Rome [6] 2006	Foissac [8] 2009	Park [18] 2017	He [15] 2020	Zhang [14] 2021	Yang [19] 2022	Cao [16] 2022	Proposed
Backpack type	Passive	Passive	Active	Active	Semi-active	Active	Active	Active
Load mass (kg)	27	16	-	19.4	25.4	16.7	20	10
Walking Speed ( $km \cdot h^{-1}$ )	5.6	3.7	3.096 ± 1.116	5.0	6.01	4.5	5.0	5.0
PA/PF reduction(%)	82% PA 33% PF	22% PA	-	98.49% PA	40% PA	-	53.2% PA	72.7%PA
Static load reduction(%)	-	-	-	-	-	-	30%	45.5%
Metabolic reduction(%)	6.2%	3.8%	8.7%	10.9%	-	15.9%	16.4%	18.68%

(SD) for the net metabolic rate were calculated for each condition. To assess the impact across different conditions, a one-way analysis of variance (ANOVA) was conducted, with a significance level set at  $\alpha = 0.05$ . These statistical analyses were performed using MATLAB. Additional details on the experimental setup specific procedures, and the obtained results will be further analyzed in the upcoming sections.

B. Walking on Treadmill

During this session, participants engaged in loaded walking tests on a treadmill set at a speed of  $5 km \cdot h^{-1}$ . Each

experimental trial included two distinct conditions:

1) 1-Min Quiet Standing Condition: Participants were required to stand quietly for a duration of 1 minute.

2) 6-Min Loaded Treadmill-Walking Tests: Subsequently, participants underwent a 6-minute session of walking on the treadmill while carrying the designated load-transfer backpack with a 10kg-load.

Fig. 12 and Table III presents a comprehensive overview of the shoulder pressure  $f_e$ , load acceleration  $\ddot{x}_2$ , and gross metabolic reduction across different experimental conditions. Notably, the ACTIVE-LLS case exhibited superior

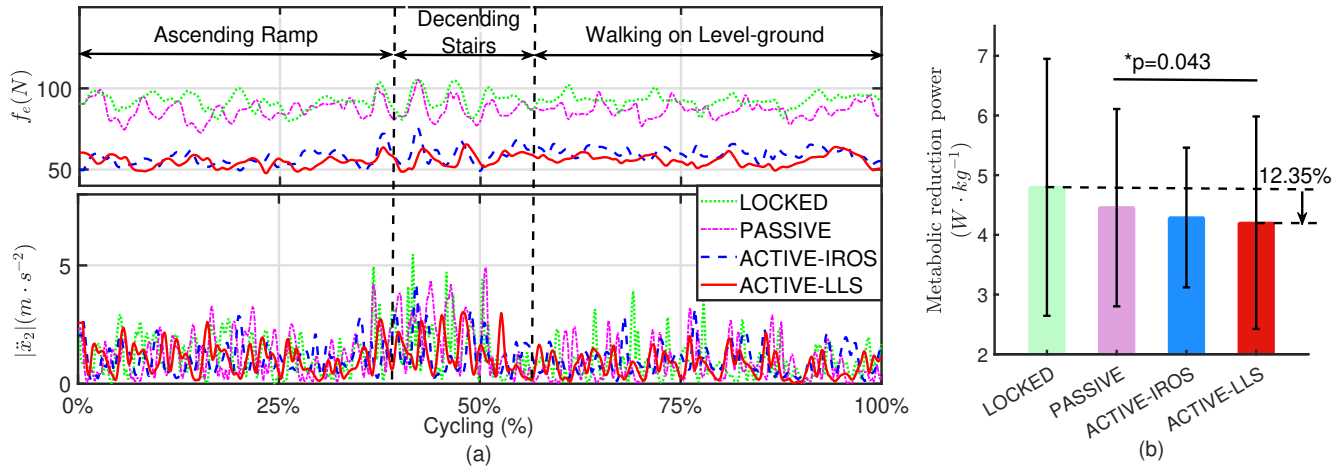


Fig. 14. Time evolution of human walking in the complex terrain. (a) Shoulder pressure and vertical load acceleration. (b) Gross metabolic reduction.

performance across all indicators, while the PASSIVE case demonstrated improved outcomes compared to the LOCKED case. Comparing the ACTIVE-LLS and PASSIVE cases, the ACTIVE-LLS configuration resulted in significant improvements. Specifically, the ACTIVE-LLS case showcased a remarkable 46.83% reduction in dynamic load-related shoulder pressures, accompanied by a corresponding 38.04% decrease in static load-related pressures. Moreover, the ACTIVE-LLS case yielded a substantial 72.7% and 62.01% reduction in maximum absolute load PA when compared to the LOCKED and the PASSIVE cases. In terms of metabolic reduction, the proposed method showcased a reduction of  $12.57\% \pm 4.68\%$  compared to the PASSIVE case, and a reduction of  $18.68\% \pm 14.15\%$  compared to the LOCKED case. These findings strongly indicate that the ACTIVE-LLS case significantly mitigated upper body stress from both a static and dynamic load perspective, contributing to a heightened sense of relaxation and concurrently promoting improved metabolic efficiency among the subjects.

Most of the current researches on suspended backpacks were focused on walking on a treadmill, and researchers have put tremendous efforts in practical experiments in [6], [8], [14], [15], [16], [18], and [19], chronologically. For this scenario, Table IV demonstrated the significance of static load transfer and dynamic load reduction for improving human locomotion capacity and enhancing metabolic efficiency. It is shown that active backpacks play a crucial role in managing load movement, yielding notable benefits in mitigating PA/PF. Concerning the active backpacks, the proposed method involves a trade-off: sacrificing a portion of the PA reduction performance to accommodate diverse application scenarios. This approach can notably improve metabolic efficiency during human load carriage by incorporating load transfer and vibration isolation, while also offering the versatility to function effectively across various terrains.

### C. Ascending Stairs

In this session, participants were requested to ascend four floors using the load-transfer backpack with a 10kg-load. Each

floor consists of 28 steps, and the ascent involved a total of 112 steps, each approximately 15 cm in height. Similar to the previous experiment, participants were instructed to stand quite for 1 minute for calculating the increment of metabolic rate. To ensure safety, participants ascended each step with a deliberate pace, taking around 0.7 seconds per step. Despite the controlled pace, the aim was to maintain a consistent speed throughout the ascent, enabling participants to complete one floor in approximately 30 seconds.

The outcomes are illustrated in Fig. 13 and Table III. Primarily, in comparison to walking on level ground, ascending stairs resulted in notably elevated shoulder pressure due to the increased foot strides necessitated by the step height. Regarding load vibrations, the ascent speed was around only  $0.21 m \cdot s^{-1}$  (equivalent to a vibration frequency of 1.1 Hz), significantly lower than the treadmill walking speed of  $1.38 m \cdot s^{-1}$  (vibration frequency of 11.74 Hz). Consequently, load vibrations were relatively subdued during this stair ascent experiment. Despite the mild vibrations, the efficacy of the system in reducing shoulder pressure can still be observed by comparing the three cases of LOCKED, PASSIVE, and ACTIVE-LLS. As indicated in Fig. 13(a), the shoulder pressure in the ACTIVE-LLS case was notably diminished compared to the PASSIVE and LOCKED cases, both in terms of vibration amplitude and bias. This reduction stems from the ACTIVE-LLS case effectively redistributing part of the load to the pelvis. Regarding the load acceleration  $\ddot{x}_2$ , the ACTIVE-LLS case displays a smaller peak load acceleration than the PASSIVE case (as depicted in Fig. 13(b)), indicating effective vibration isolation performance of the proposed method. In terms of metabolic reduction, compared to the LOCKED case, the PASSIVE case experienced a 4.98% decrease, whereas the ACTIVE-LLS case exhibited a more substantial 9.58% reduction. This underscores the system's ability to effectively alleviate shoulder pressure and enhance metabolic efficiency during load carriage in ascending stairs.

### D. Walking on Complex Terrain

The walking environment includes ramps, stairs, and level ground. The ramp features a 10-degree incline and measures about 3.45 m in length. The staircase consists of four steps, each with an approximate height of 15 cm, and there is a level ground stretch of approximately 3.3 m between the base of the stairs and the base of the ramp. In this experiment, participants were requested to complete a series of sequential walks within a single cycle: ascending the ramp, descending the staircase, and finally traversing level ground from the base of the stairs to the base of the ramp. Each cycle was expected to take approximately 16 seconds, with a total of 18 cycles. Likewise, participants were instructed to maintain a quiet stance for 1 minute to assess variations in the metabolic rate.

TABLE V  
PERFORMANCE EVALUATION IN WALKING ON COMPLEX TERRAIN

	$f_e$ (N)	MAX( $\ddot{x}_2$ ) ( $m \cdot s^{-2}$ )	Metabolic Reduction ( $W \cdot kg^{-1}$ )
LOCKED	92.48 ± 16.42	5.47	4.79 ± 2.15
PASSIVE	89.07 ± 12.54	4.92	4.46 ± 1.65
ACTIVE-IROS	62.27 ± 13.46	4.51	4.29 ± 1.17
ACTIVE-LLS	58.65 ± 8.86	3.03	4.20 ± 1.78

The results shows the time evolution of human walking in the complex terrain. Analyzing Fig. 14 and Table V, it becomes apparent that walking across diverse terrains notably influences shoulder pressure and PA. Specifically, when descending stairs, load vibrations visibly intensify, while both uphill and flat terrain result in comparable levels of load vibrations. With consistent human walking speed, this discrepancy can be attributed to the varying shifts in COG, with stairs inducing more pronounced COG changes compared to the relatively subtle changes observed on gradual slopes and flat surfaces. The ACTIVE-LLS case exhibited the smallest variations in shoulder pressure and load acceleration across all terrains, with a maximum acceleration of only  $3.0312 m \cdot s^{-2}$ , surpassing the performance of both the PASSIVE, LOCKED and ACTIVE-IROS configurations. This indicates that the LLS-type bio-inspired vibration isolator is insensitive to varying walking conditions and effectively minimizes shoulder impacts. Additionally, in comparison, the ACTIVE-IROS configuration performed similarly to the PASSIVE configuration in terms of load acceleration. This similarity arises primarily from the fact that the ACTIVE-IROS case fundamentally relies on a linear vibration isolator. While it performs well on flat ground, its effectiveness significantly decreases on complex terrains, such as descending stairs. Both the ACTIVE-LLS and ACTIVE-IROS configurations achieved similar load transfer in the experiments, resulting in similar average shoulder pressure levels. The LLS-type bio-inspired vibration isolator achieved a 34.17% reduction in shoulder pressure amplitude and a 32.64% decrease in maximum acceleration, indicating its superior capability in optimizing vibration isolation. Upon analyzing human metabolic reduction, it is evident that the LOCKED, PASSIVE, ACTIVE-IROS and ACTIVE-LLS configurations consumed  $4.7960 \pm 2.1525 W \cdot kg^{-1}$ ,  $4.4552 \pm 1.6531 W \cdot kg^{-1}$ ,  $4.2901 \pm 1.1706 W \cdot kg^{-1}$

and  $4.2035 \pm 1.7795 W \cdot kg^{-1}$ . This energy consumption aligns with the levels previously observed in the flat walking experiment and is significantly lower than in the stair climbing experiment. In addition, the metabolic efficiency increased by an average of 10.55% for the ACTIVE-IROS configuration and 12.35% for the ACTIVE-LLS configuration, compared to the LOCKED configuration. This improvement highlights the effectiveness of the proposed methodology in enhancing the metabolic efficiency of load carriage across various terrains.

### E. Discussion

The main goal of this paper is to validate the performance of the active load-transfer backpack across various terrains, using a fixed desired load transfer ratio regardless of terrain,  $\xi_d = 0.5$ . Although this approach may not achieve a perfectly balanced load distribution between the shoulders and pelvis across diverse terrains, it still facilitates load transfer and improves metabolic efficiency. While we recognize that this fixed ratio may not be optimal, it was chosen for the following reasons: 1) The aforementioned analysis suggests that partial load transfer can enhance metabolic energy efficiency during load carriage (for further details, please refer to Remark 2). 2) Accurately controlling the load distribution between the shoulders and pelvis is challenging in practical applications due to factors such as torso inclination, muscle strength, terrain, and movement dynamics. 3) Because human metabolic energy consumption is affected by both subjective and objective factors and varies widely among individuals, a large sample size is required to ensure statistical significance in the experiment. Overall, determining the optimal load distribution ratios for enhancing human metabolic energy efficiency across different terrains remains an open issue.

The presented LLS-type dynamic models can accurately represent physical LLS-type bio-inspired vibration isolators because they are built based on the physical laws, particularly Lagrangian equations. These models simulate the behavior of physical systems by capturing mechanical characteristics and have been validated in numerous studies [22], [26], [28]. Meanwhile, physical vibration isolators are often constrained by fixed structural parameters and are susceptible to non-ideal factors such as friction, assembly errors, and uneven mass distribution. Moreover, physical vibration isolators require extra mechanical structures to facilitate load transfer, which adds to both design complexity and system mass. This can potentially hinder portability and impose a greater burden on human shoulders. In contrast, the proposed method eliminates these constraints, allowing for flexible performance adjustments while significantly reducing both time and cost.

This study primarily focuses on a 10kg-load specifically designed for the active suspended backpack. This choice is driven by two main reasons: 1) The primary focus of our application is on carrying scenarios in complex terrains, where an excessively heavy load could compromise both the safety and mobility of the human-robot system. 2) The LLS-type bio-inspired vibration isolation model was specifically designed for a 10kg-load, optimizing the system's performance. Using different load masses can affect the vibration isolator's

performance, including its vibration isolation effectiveness and the human metabolic energy efficiency. Consequently, at this stage, we primarily focused on validating the system's performance with a 10kg-load. Future work will focus on investigating how varying load masses affect vibration isolation performance, with a key challenge being the development of a method to dynamically adjust the vibration isolator's parameters in real-time, ensuring optimal performance across a wide range of load.

While field experiments on rugged mountainous terrain were explored as part of future perspectives and showed preliminary promising results (with the detailed experimental procedure provided in the multimedia), we chose to focus on controlled laboratory conditions for the current study due to the numerous uncertainties and uncontrollable factors in the field environment, such as the complexity of ground conditions, uncontrolled ambient temperatures, changing weather conditions, and variability in human walking. These factors made it challenging to precisely quantify the experimental conditions and to ensure the reliability of the results, potentially compromising the scientific rigor and generalizability.

## VII. CONCLUSION

This paper introduces a novel load-transfer suspended backpack integrated with a Lagrangian-based bio-inspired vibration isolator, aiming to alleviate human shoulder pressure and enhance metabolic efficiency during load carriage. The approach is founded on the double-mass coupled-oscillator model, presenting a comprehensive control framework encompassing both a reference generator and a position controller. The reference generator is derived from the combination of the load-transfer principle and an LLS-type bio-inspired vibration isolator. This ensures optimized load distribution and vibration isolation. Next, an SEA-based controller with prescribed performance is employed to achieve position tracking and guarantee the load operates within the travel range. The theoretical foundation asserts the input-output stability of the bio-inspired vibration isolator and the ultimate uniform boundedness of the closed-loop system. Simulations and real-world experiments conducted across diverse scenarios validate the effectiveness of the proposed method. Results consistently showcase the substantial reduction of pressure on the human shoulder, coupled with improvements in human metabolic efficiency throughout various load carriage scenarios.

In the future, we will build a human biomechanics model and assess the mechanical work performed by muscles during various walking patterns to quantitatively analyze the impact of load distribution on metabolic consumption. This approach involves numerous muscles in both the upper and lower body, necessitating extensive collection of physiological signals. These include electromyography signals from muscles such as the erector spinae in the upper back, deltoids in the shoulders, rectus abdominis in the abdomen, as well as quadriceps, hamstrings, etc. in the lower body. Additionally, data on limb and trunk movements, foot pressure, joint angles and other metrics, would be required. This may comprehensively and quantitatively analyze the objective factors influencing energy

consumption during load carriage, aiming to establish the optimal load distribution between the shoulders and pelvis.

## APPENDIX

### PROOF OF THE LEMMA 1

A Lyapunov candidate is defined as:

$$V_p = \frac{1}{2} \begin{bmatrix} Y_1 & Y_2 \end{bmatrix} \begin{bmatrix} \frac{\lambda_y c_1 + k_v}{m_2} & \lambda_y \\ \frac{c_1}{m_2} & 1 \end{bmatrix} \begin{bmatrix} Y_1 \\ Y_2 \end{bmatrix} \quad (50)$$

$$+ \frac{k_h}{2m_2} \int_0^{Y_1} d_h \Psi_1 d\xi + \frac{\lambda_y}{m_2} \int_0^{Y_1} f(\Psi_0, \Psi_1) Y_1 d\xi.$$

where  $\lambda_y$  is a positive constant.  $f(\Psi_0, \Psi_1) = \frac{c_h}{4} \Psi_1^2 + \frac{c_3 n_x}{4L_1^2} \Psi_0^2 \geq 0$ . As the isolator works within the range of the positive-only stiffness, we have  $V_p \geq 0$ . Hence, the derivative of  $V_p$  is denoted as:

$$\dot{V}_p = \frac{\lambda_y c_1 + k_v}{m_2} Y_1 Y_2 + \frac{1}{2} \left( \frac{c_1}{m_2} + \lambda_y \right) \left( Y_2^2 + Y_1 \dot{Y}_2 \right) + Y_2 \dot{Y}_2 \quad (51)$$

$$+ \frac{k_h}{2m_2} d_h \Psi_1 Y_2 + \frac{\lambda_y}{m_2} f(\Psi_0, \Psi_1) Y_1 Y_2$$

Let  $\lambda_y = \frac{c_1}{m_2}$ . By substituting (26) into (51), we obtain:

$$\dot{V}_p = -\frac{\lambda_y k_v}{m_2} Y_1^2 - \frac{\lambda_y k_h}{2m_2} d_h Y_1 \Psi_1 - \frac{f(\Psi_0, \Psi_1)}{m_2} Y_2^2 \quad (52)$$

$$+ (\lambda_y Y_1 + Y_2) U$$

Due to  $\varphi_i$  is operating within the range of  $(0, \frac{\pi}{2} - \theta_i)$ , the following equations hold, as  $\frac{d_i}{L_i} = \cos(\theta_i) - \cos(\theta_i + \varphi_i)$  and  $\frac{Y_1}{2L_i} = \frac{y}{2L_i} = \frac{h}{L_i} = \sin(\theta_i + \varphi_i) - \sin(\theta_i)$  according to (12).

$$\frac{Y_1 d_i}{2L_i^2} = \sin(2\theta_i + \varphi_i) - \frac{1}{2}(\sin(2\theta_i) + \sin(2\theta_i + 2\varphi_i)) \quad (53)$$

$$= \sin(2\theta_i + \varphi_i)(1 - \cos(\varphi_i)) \geq 0,$$

$$\Rightarrow d_h Y_1 = (d_1 + d_2) Y_1 \geq 0$$

Note that  $\frac{\partial d_h}{\partial y} = \frac{1}{2} \Psi_1 \geq 0$ , the following equality holds:

$$\dot{V}_p \leq -\frac{\lambda_y k_v}{m_2} Y_1^2 - \frac{f(\Psi_0, \Psi_1)}{m_2} Y_2^2 + (\lambda_y Y_1 + Y_2) U \quad (54)$$

$$= -\left( \frac{\lambda_y k_v}{m_2} - \eta \lambda_y^2 \right) Y_1^2 - \left( \frac{f(\Psi_0, \Psi_1)}{m_2} - \eta \right) Y_2^2$$

$$- \eta \lambda_y^2 Y_1^2 - \eta Y_2^2 + (\lambda_y Y_1 + Y_2) U$$

$$\leq -\left( \frac{\lambda_y k_v}{m_2} - \eta \lambda_y^2 \right) Y_1^2 - \left( \frac{f(\Psi_0, \Psi_1)}{m_2} - \eta \right) Y_2^2$$

$$- \frac{\eta}{2} \|\vec{Y}\|_2^2 + \sqrt{2} \|\vec{Y}\|_2 |U|$$

$$\leq -\left( \frac{\lambda_y k_v}{m_2} - \eta \lambda_y^2 \right) Y_1^2 - \left( \frac{f(\Psi_0, \Psi_1)}{m_2} - \eta \right) Y_2^2,$$

$$\forall \|\vec{Y}\|_2 \geq \frac{2\sqrt{2}|U|}{\eta}$$

where  $0 < \eta < \min\left(\frac{k_v}{c_1}, \frac{f(\Psi_0, \Psi_1)}{m_2}\right)$  and  $\vec{Y} = [\lambda_y Y_1, Y_2]^T$ . Since  $V_p$  is positive definite and radially unbounded. Hence, the system is input-to-state stable. Furthermore, the function  $Y = Y_1 = y$  satisfied  $Y \leq \alpha_1(\|\vec{Y}\|) + \alpha_2(U) + \alpha_3$  globally with the class  $\mathcal{K}$  functions  $\alpha_1(\|\vec{Y}\|) = \frac{\sqrt{2}}{\lambda_y} \|\vec{Y}\|, \alpha_2(U) =$

0 and a nonnegative constant  $\alpha_3$ . Thus, the LLS-type bio-inspired vibration isolator is  $L_\infty$  stable from  $(U, Y)$ .

This completes the proof.

#### APPENDIX PROOF OF THE THEOREM 1

A Lyapunov candidate function is defined as:

$$V_x = \frac{1}{2}m_2\sigma_x^2 + \tilde{\phi}_x^T \frac{1}{2\Gamma_x} \tilde{\phi}_x \quad (55)$$

Differentiating (55) with respect to time, it follows that

$$\begin{aligned} \dot{V}_x &= \sigma_x m_2 \dot{\sigma}_x + \tilde{\phi}_x^T \frac{1}{\Gamma_x} \dot{\tilde{\phi}}_x \\ &= \sigma_x (-c_\rho \sigma_x - \kappa_x \sigma_x - \Lambda(x_\rho, \dot{x}_r, \ddot{x}_r)^T \tilde{\phi}_x \\ &\quad + f_\rho + \nu_\rho + k_\tau l_b \Delta \theta) + \sigma_x \Lambda(x_\rho, \dot{x}_r, \ddot{x}_r)^T \tilde{\phi}_x \\ &= -(c_\rho + \kappa_x) \sigma_x^2 + (f_\rho + \nu_\rho + k_\tau l_b \Delta \theta) \sigma_x \end{aligned} \quad (56)$$

Defining another Lyapunov candidate function, we have

$$V_c = V_x + \frac{1}{2}J\sigma_\theta^2 + \tilde{\phi}_\theta^T \frac{1}{2\Gamma_\theta} \tilde{\phi}_\theta + \kappa_{\theta 2} \lambda_\theta \Delta \theta^2 \quad (57)$$

the derivative is expressed as:

$$\begin{aligned} \dot{V}_c &= \dot{V}_x + \sigma_\theta (-\kappa_\theta \sigma_\theta - b\sigma_\theta - \Lambda(\dot{\theta}_r, \ddot{\theta}_r)^T \tilde{\phi}_\theta + \nu_\tau) \\ &\quad + \sigma_\theta \Lambda(\dot{\theta}_r, \ddot{\theta}_r)^T \tilde{\phi}_\theta + 2\kappa_{\theta 2} \lambda_\theta \Delta \theta \dot{\Delta} \theta \\ &= -(c_\rho + \kappa_x) \sigma_x^2 + (f_\rho + k_\tau l_b \Delta \theta + \nu_\rho) \sigma_x \\ &\quad - (\kappa_{\theta 1} + \kappa_{\theta 2} + b) \sigma_\theta^2 + \nu_\tau \sigma_\theta + 2\kappa_{\theta 2} \lambda_\theta \Delta \theta \dot{\Delta} \theta \\ &= (f_\rho + \nu_\rho) \sigma_x + \nu_\tau \sigma_\theta - (c_\rho + \kappa_x) \sigma_x^2 - (\kappa_{\theta 1} + b) \sigma_\theta^2 \\ &\quad + k_\tau l_b \Delta \theta \sigma_x - \kappa_{\theta 2} \Delta \dot{\theta}^2 - \kappa_{\theta 2} \lambda_\theta^2 \Delta \theta^2 \\ &= (f_\rho + \nu_\rho) \sigma_x + \nu_\tau \sigma_\theta - (\kappa_{\theta 1} + b) \sigma_\theta^2 - \kappa_{\theta 2} \Delta \dot{\theta}^2 \\ &\quad - \begin{bmatrix} \sigma_x & \Delta \theta \end{bmatrix} \begin{bmatrix} c_\rho + \kappa_x & -\frac{1}{2}k_\tau l_b \\ -\frac{1}{2}k_\tau l_b & \kappa_{\theta 2} \lambda_\theta^2 \end{bmatrix} \begin{bmatrix} \sigma_x \\ \Delta \theta \end{bmatrix} \end{aligned} \quad (58)$$

Let  $s = \begin{bmatrix} \sigma_x & \Delta \theta \end{bmatrix}^T$ ,  $P_1 = \begin{bmatrix} c_\rho + \kappa_x & -\frac{1}{2}k_\tau l_b \\ -\frac{1}{2}k_\tau l_b & \kappa_{\theta 2} \lambda_\theta^2 \end{bmatrix}$ , then  $s^T P_1 s > 0$  according to (44).

Hence, treating  $f_\rho$  as the input to the system, while considering  $\sigma_x$  as the output, the system presents passivity with  $\nu_\rho = 0, \nu_\tau = 0$  and time integral over  $[0, t]$  is denoted as:

$$\begin{aligned} \int_0^t f_\rho \sigma_x d\xi &= \int_0^t W_{loss}^x d\xi + V_c(t) - V_c(0) \\ &\geq V_c(t) - V_c(0) \end{aligned} \quad (59)$$

where  $W_{loss}^x = (\kappa_{\theta 1} + b) \sigma_\theta^2 + \kappa_{\theta 2} \Delta \dot{\theta}^2 + s^T P_1 s \geq 0$ .

This completes the proof.

#### APPENDIX PROOF OF THE THEOREM 2

From (58), we have the following relationship:

$$\begin{aligned} \dot{V}_c &\leq f_m^2 + \bar{\nu}_\rho^2 + \bar{\nu}_\tau^2 + \frac{1}{2}\sigma_x^2 + \frac{1}{4}\sigma_\theta^2 - (c_\rho + \kappa_x) \sigma_x^2 \\ &\quad - (\kappa_{\theta 1} + b) \sigma_\theta^2 + k_\tau l_b \Delta \theta \sigma_x - \kappa_{\theta 2} \Delta \dot{\theta}^2 - \kappa_{\theta 2} \lambda_\theta^2 \Delta \theta^2 \\ &= f_m^2 + \bar{\nu}_\rho^2 + \bar{\nu}_\tau^2 - (\kappa_{\theta 1} + b - \frac{1}{4}) \sigma_\theta^2 - \kappa_{\theta 2} \Delta \dot{\theta}^2 - s^T P_2 s \\ &\leq -\lambda_{\min}(P_2) \|s\|^2 + f_m^2 + \bar{\nu}_\rho^2 + \bar{\nu}_\tau^2 \end{aligned} \quad (60)$$

where  $P_2 = \begin{bmatrix} c_\rho + \kappa_x - \frac{1}{2} & -\frac{1}{2}k_\tau l_b \\ -\frac{1}{2}k_\tau l_b & \kappa_{\theta 2} \lambda_\theta^2 \end{bmatrix}$  is positive definite. Thus, the absolute value of  $\sigma_x$  is bounded by

$$|\sigma_x| \leq \|s\| \leq \sqrt{\frac{f_m^2 + \bar{\nu}_\rho^2 + \bar{\nu}_\tau^2}{\lambda_{\min}(P_2)}} \quad (61)$$

By defining another Lyapunov candidate function  $V_z = \frac{1}{2}z^2$ , its derivative respect to time is:

$$\begin{aligned} \dot{V}_z &= z\dot{z} = z(\sigma_z - \lambda_z z) = -\lambda_z z^2 + z \frac{\sigma_x}{\vartheta_1} \\ &= -z(\lambda_z z - \frac{\sigma_x}{\vartheta_1}) \end{aligned} \quad (62)$$

Hence, the transformed tracking error  $z$  is bounded by:

$$|z| \leq \frac{1}{\lambda_z \vartheta_1} \sqrt{\frac{f_m^2 + \bar{\nu}_\rho^2 + \bar{\nu}_\tau^2}{\lambda_{\min}(P_2)}} \quad (63)$$

This completes the proof.

#### REFERENCES

- [1] D. Chow, M. Kwok, A. Au-Yang, A. Holmes, J. Cheng, F. Yao & M. Wong, "The effect of backpack load on the gait of normal adolescent girls," *Ergonomics*, vol. 48, no. 6, pp. 642-656, 2005.
- [2] P. Quesada, L. Mengelkoch, R. Hale, and S. Simon, "Biomechanical and metabolic effects of varying backpack loading on simulated marching," *Ergonomics*, vol. 43, no. 3, pp. 293-309, 2000.
- [3] R. Kram, "Carrying loads with springy poles," *J. Appl. Physiol.*, vol. 71, no. 3, pp. 1119-1122, 1991.
- [4] J. Ackerman and J. Seipel, "Energy Efficiency of Legged Robot Locomotion With Elastically Suspended Loads," *IEEE Trans. Robot.*, vol. 29, no. 2, pp. 321-330, April 2013.
- [5] E. R. Castillo, G. M. Lieberman, L. S. McCarty and D. E. Lieberman, "Effects of pole compliance and step frequency on the biomechanics and economy of pole carrying during human walking," *J. Appl. Physiol.*, vol. 117, no. 5, pp. 507-517, 2014.
- [6] L. Rome, L. Flynn and T. Yoo, "Rubber bands reduce the cost of carrying loads," *Nature*, vol. 444, pp. 1023-1024, 2006.
- [7] J. Liang, Q. Zhang, Y. Liu, et al. "A review of the design of load-carrying exoskeletons," *Sci. China Technol. Sci.*, vol. 65, pp. 2051-2067, 2022.
- [8] M. Foissac, G. Y. Millet, A. Geysant, P. Freychat, A. Belli, "Characterization of the mechanical properties of backpacks and their influence on the energetics of walking," *J. Biomech.*, vol. 42, no. 2, pp. 125-130, 2009.
- [9] H. Li, D. Sui, H. Ju, Y. An, J. Zhao and Y. Zhu, "Mechanical Compliance and Dynamic Load Isolation Design of Lower Limb Exoskeleton for Locomotion Assistance," *IEEE-ASME Trans. Mechatron.*, vol. 27, no. 6, pp. 5392-5402, Dec. 2022.
- [10] Y. Leng et al., "Design and Implement an Elastically Suspended Back Frame for Reducing the Burden of Carrier," *Proc. IEEE Int. Conf. Adv. Robot. Mechatron. (ICARM)*, Chongqing, China, 2021, pp. 236-240.
- [11] J. Ackerman and J. Seipel, "A model of human walking energetics with an elastically-suspended load," *J. Biomech.*, vol. 47, no. 8, pp. 1922-1927, 2014.
- [12] L. Yang, Y. Xu, J. Zhang, K. Chen and C. Fu, "Design of an Elastically Suspended Backpack with a Tunable Damper," *Proc. IEEE Int. Conf. Adv. Robot. Soc. Impacts (ARSO)*, Beijing, China, 2019, pp. 180-185.
- [13] B. Zhang, Y. Liu, W. Fan, Z. Wang and T. Liu, "Pilot Study of a Hover Backpack with Tunable Air Damper for Decoupling Load and Human," *Proc. IEEE/ASME Int. Conf. Adv. Intell. Mechatron. (AIM)*, Boston, MA, USA, 2020, pp. 1834-1839.
- [14] B. Zhang, T. Liu, W. Fan and J. Zhang, "Sliding Mode Control of the Semi-active Hover Backpack Based on the Bioinspired Skyhook Damper Model," *Proc. IEEE Int. Conf. Robot. Autom. (ICRA)*, Xi'an, China, 2021, pp. 9389-9395.
- [15] L. He, C. Xiong, Q. Zhang, W. Chen, C. Fu and K. -M. Lee, "A Backpack Minimizing the Vertical Acceleration of the Load Improves the Economy of Human Walking," *IEEE Trans. Neural Syst. Rehabil. Eng.*, vol. 28, no. 9, pp. 1994-2004, Sept. 2020.

- [16] Y. Cao et al., "Metabolic Efficiency Improvement of Human Walking by Shoulder Stress Reduction through Load Transfer Backpack," *Proc. IEEE/RSJ Int. Conf. Intell. Robots Syst. (IROS)*, Kyoto, Japan, 2022, pp. 3934-3939.
- [17] Z. Yang, L. Huang, Z. Zeng, R. Wang, R. Hu, L. Xie, "Evaluation of the Load Reduction Performance Via a Suspended Backpack With Adjustable Stiffness," *J. Biomech. Eng.*, vol. 14, no. 5, pp. 051001, May 2022.
- [18] J. -H. Park, P. Stegall, H. Zhang and S. Agrawal, "Walking With a Backpack Using Load Distribution and Dynamic Load Compensation Reduces Metabolic Cost and Adaptations to Loads," *IEEE Trans. Neural Syst. Rehabil. Eng.*, vol. 25, no. 9, pp. 1419-1430, Sept. 2017.
- [19] L. Yang, C. Xiong, M. Hao, Y. Leng, K. Chen and C. Fu, "Energetic Response of Human Walking With Loads Using Suspended Backpacks," *IEEE-ASME Trans. Mechatron.*, vol. 27, no. 5, pp. 2973-2984, Oct. 2022.
- [20] Y. Leng, X. Lin, L. Yang, K. Zhang, X. Chen and C. Fu, "A Model for Estimating the Leg Mechanical Work Required to Walk With an Elastically Suspended Backpack," *IEEE Trans. Hum.-Mach. Syst.*, vol. 52, no. 6, pp. 1303-1312, Dec. 2022.
- [21] Z. Wu, X. Jing, J. Bian, F. Li and R. Allen, "Vibration isolation by exploring bio-inspired structural nonlinearity," *Bioinspir. Biomim.*, vol. 10, no. 5, pp. 056015, 2015.
- [22] G. Yan, H.-X. Zou, S. Wang, L.-C. Zhao, Z.-Y. Wu, W.-M. Zhang, "Bio-Inspired Vibration Isolation: Methodology and Design," *Appl. Mech. Rev.*, vol. 73, no. 2, pp. 020801, 2021.
- [23] X. Jing, "The X-structure/mechanism approach to beneficial nonlinear design in engineering," *Appl. Math. Mech.-Engl. Ed.* vol. 43, pp. 979-1000, 2022.
- [24] J. Bian, X. Jing, "Superior nonlinear passive damping characteristics of the bio-inspired limb-like or X-shaped structure," *Mech. Syst. Signal Proc.*, vol. 125, no. 15, pp. 21-51, June 2019.
- [25] M.-Q. Niu, L. Chen, "Analysis of a bio-inspired vibration isolator with a compliant limb-like structure," *Mech. Syst. Signal Proc.*, vol. 179, no. 1, pp. 109348, Nov. 2022.
- [26] M. Zhang, X. Jing and G. Wang, "Bioinspired Nonlinear Dynamics-Based Adaptive Neural Network Control for Vehicle Suspension Systems With Uncertain/Unknown Dynamics and Input Delay," *IEEE Trans. Ind. Electron.*, vol. 68, no. 12, pp. 12646-12656, Dec. 2021.
- [27] X. Hu, G. Wen, S. Yin, et al., "Approximation-free control based on the bioinspired reference model for suspension systems with uncertainty and unknown nonlinearity," *Nonlinear Dyn.*, vol. 111, pp. 3149-3171, 2023.
- [28] H. Pan, X. Jing, W. Sun and H. Gao, "A Bioinspired Dynamics-Based Adaptive Tracking Control for Nonlinear Suspension Systems," *IEEE Trans. Control Syst. Technol.*, vol. 26, no. 3, pp. 903-914, May 2018.
- [29] M. Perrone, R. Orr, W. Hing, N. Milne and R. Pope, "The Impact of Backpack Loads on School Children: A Critical Narrative Review," *Int. J. Environ. Res. Public Health*, vol. 15, pp. 2529, 2018.
- [30] T. Li, Q. Li, "A systematic review on load carriage assistive devices: Mechanism design and performance evaluation," *Mech. Mach. Theory*, vol. 180, pp. 105142, Feb. 2023.
- [31] D. Wang, K. -M. Lee and J. Ji, "A Passive Gait-Based Weight-Support Lower Extremity Exoskeleton With Compliant Joints," *IEEE Trans. Robot.*, vol. 32, no. 4, pp. 933-942, Aug. 2016
- [32] W. van Dijk et al., "Exobuddy - A Non-Anthropomorphic Quasi-Passive Exoskeleton for Load Carrying Assistance," *Proc. IEEE Int. Conf. Biomed. Robot. Biomechatron. (BioRob)*, Enschede, Netherlands, 2018, pp. 336-341.
- [33] Z. Zhou, W. Chen, H. Fu, X. Fang and C. Xiong, "Design and Experimental Evaluation of a Nonanthropomorphic Passive Load-carrying Exoskeleton," *Proc. IEEE Int. Conf. Adv. Robot. Mechatronics (ICARM)*, Chongqing, China, 2021, pp. 251-256.
- [34] Ming Hao, Jiwen Zhang, Ken Chen, Harry Asada, Chenglong Fu, "Supernumerary Robotic Limbs to Assist Human Walking With Load Carriage," *J. Mechanisms Robotics*, vol. 12, no. 6, pp. 061014, Dec. 2020.
- [35] K. N. Gregorczyk, L. Hasselquist, J. M. Schiffman, C. K. Bensek, J. P. Obusek, D. J. Gutekunst, "Effects of a lower-body exoskeleton device on metabolic cost and gait biomechanics during load carriage," *Ergonomics*, vol. 53, pp. 1263-1275, 2010.
- [36] Joon-Hyuk Park, Xin Jin, Sunil K. Agrawal, "Second Spine: Upper Body Assistive Device for Human Load Carriage," *J. Mechanisms Robotics*, vol. 7, no. 1, pp. 011012, Feb 2015.
- [37] C. P. Bechlioulis and G. A. Rovithakis, "Prescribed performance adaptive control of SISO feedback linearizable systems with disturbances," *Proc. 16th Mediterranean Conf. Control Autom.*, Ajaccio, France, 2008, pp. 1035-1040
- [38] Y. Cao, M. Zhang, J. Huang and S. Mohammed, "Prescribed performance control of a link-type exoskeleton powered by pneumatic muscles with virtual elasticity," *Nonlinear Dyn.* vol. 112, pp. 10043-10060, 2024.
- [39] M. Zhang, Y. Cao, J. Huang, X. Chen, "Cross-backstepping control with prescribed performance for input-coupled underactuated systems under arbitrary initial conditions," *J. Frankl. Inst.*, vol. 360, no. 16, pp. 11892-11915, 2023.
- [40] L. Zheng et al., "3D Navigation Control of Untethered Magnetic Micro-robot in Centimeter-Scale Workspace Based on Field-of-View Tracking Scheme," *IEEE Trans. Robot.*, vol. 38, no. 3, pp. 1583-1598, June 2022.
- [41] Y. Cao, X. Chen, M. Zhang and J. Huang, "Adaptive Position Constrained Assist-As-Needed Control for Rehabilitation Robots," *IEEE Trans. Ind. Electron.*, 2023, vol. 71, no. 4, pp. 4059-4068, April 2024.
- [42] D. Papageorgiou, T. Kastritsi, Z. Doulgeri and G. A. Rovithakis, "A Passive pHRI Controller for Assisting the User in Partially Known Tasks," *IEEE Trans. Robot.*, vol. 36, no. 3, pp. 802-815, June 2020.
- [43] S. Wang, B. Zhang, Z. Yu and Y. Yan, "Differential Soft Sensor-Based Measurement of Interactive Force and Assistive Torque for a Robotic Hip Exoskeleton," *Sensors*, vol. 21, no. 19, pp. 6545, 2021.
- [44] S. Ulman, D. Srinivasan and M. A. Nussbaum, "Task demand and load carriage experience affect gait variability among military cadets," *Sci. Rep.*, vol. 12, Article number: 18347, 2022.
- [45] S. Chatterjee, T. Chatterjee, D. Bhattacharyya, S. Sen, and M. Pal, "Effect of heavy load carriage on cardiorespiratory responses with varying gradients and modes of carriage," *Military Med. Res.*, vol. 5, no. 26, 2018.
- [46] M. Lafiandra and E. Harman, "The distribution of forces between the upper and lower back during load carriage," *Med. Sci. Sports Exerc.*, vol. 36, no. 3, pp. 460-467, 2004.
- [47] A. Grabowski, C. T. Farley, and R. Kram, "Independent metabolic costs of supporting body weight and accelerating body mass during walking," *J. Appl. Physiol.* vol. 98, no. 2, pp. 579-583, 2005.
- [48] J. G. Grenier, N. Peyrot, J. Castells, et al. "Energy cost and mechanical work of walking during load carriage in soldiers," *Med. Sci. Sports Exerc.*, vol. 44, no. 6, pp. 1131-1140, 2012.



**Yu Cao** (S'17-M'21) received the B.S. degree in automation from Wuhan University of Technology, Wuhan, China, in 2011, the M.E degree in software engineering and Ph.D degree in control science and engineering from Huazhong University of Science and Technology, Wuhan, China in 2014 and 2020, respectively. From 2021.1-2024.3, he was a Postdoctoral Researcher at the School of Artificial Intelligence and Automation, Huazhong University of Science and Technology.

He received funding from the Marie Skłodowska-Curie Actions, supported by UKRI under the Horizon Europe Guarantee in 2023, and he currently is a UKRI Research Fellow in Rehabilitation Robotics at the School of Electronic & Electrical Engineering, Faculty of Engineering & Physical Sciences, University of Leeds, Leeds, UK. His current research interests include human-robot interaction control, neuromusculoskeletal modelling, and wearable robotic systems.



**Mengshi Zhang** received the B.S. degree in automation from South-Central University for Nationalities, Wuhan, China, in 2017, and received the Ph.D. degree in control science and engineering with the School of Artificial Intelligence and Automation, Huazhong University of Science and Technology, Wuhan, China, in 2023.

She is currently a Robotics System Engineer at Wuhan United Imaging Healthcare Surgical Technology Co., Ltd., working on the development of surgical robots. Her current research interests include surgical robotics, servo driver design, and human-robot interaction control.



**Jian Huang** (M'07-SM'17) graduated in automatic control from the Huazhong University of Science and Technology (HUST), Wuhan, China, in 1997, and received the M.E. degree in control theory and control engineering and Ph.D. degree in control science and engineering from HUST, in 2000 and 2005, respectively.

From 2006 to 2008, he was a Postdoctoral Researcher at the Department of Micro-Nano System Engineering and the Department of Mechano-Informatics and Systems, Nagoya University, Japan.

He is currently a Full Professor with the School of Artificial Intelligence and Automation, HUST. His main research interests include rehabilitation robot, robotic assembly, networked control systems and bioinformatics.



**Samer Mohammed** (Senior Member, IEEE) received the Ph.D. degree from University of Montpellier - LIRMM/CNRS, Montpellier, France, in 2006, and the Habilitation to supervise research degree in robotics from the University of Paris-Est Creteil, Creteil, France, in 2016.

He is currently a Full Professor with University Paris-Est Creteil. He has authored or coauthored more than 100 papers in scientific journals, books, and conference proceedings. His research interests include modeling and control of robotic systems (wearable robots), artificial intelligence, and decision-support theory with target applications on the functional assisting of dependent people. Dr. Mohammed is the General Chair of the IEEE-RAS Technical Committee on Wearable Robotics. He co-organized many national and international workshops and conferences in the field of wearable technologies.